EE-ASTN-1827

Final Report

LIQUID PHASE SINTERED COMPACTS IN SPACE

September 1974

TELEDYNE
BROWN ENGINEERING

Cummings Research Park • Huntsville, Alabama 35807

FINAL REPORT
EE-ASTN-1827

LIQUID PHASE SINTERED COMPACTS IN SPACE

By

T. K. Mookherji, Ph.D.
W. B. McAnelly, Ph.D.

September 1974

Prepared For

SCIENCE AND ENGINEERING
GEORGE C. MARSHALL SPACE FLIGHT CENTER
HUNTSVILLE, ALABAMA

Contract No. NAS8-29951

Prepared By

RESEARCH LABORATORIES
ELECTRONICS AND ENGINEERING
TELEDYNE BROWN ENGINEERING
HUNTSVILLE, ALABAMA

ABSTRACT

A model that will explain the effect of gravity on liquid phase sintering has been developed. Wetting characteristics and density segregation which are the two important phenomena in liquid phase sintering are considered for the model development.

Experiments were also conducted on some selected material combinations to study the gravity effects on liquid phase sintering and also to verify the validity of the model.

It is concluded that

- The surface tension forces acting on solid particles in a one-g environment are not appreciably different from those anticipated in a 10^{-5} g/g_0 (or lower) environment.
- The capillary forces are dependent on the contact angle, the quantity of the liquid phase, and the distance between solid particles. Even for moderate angles of contact, the attractive force can be converted to repulsive force by varying the quantity of the liquid phase.
- The pores (i.e., bubbles) do not appear to be driven to the surface by gravity-produced buoyancy forces.
- The length of time to produce the same degree of settling in a low-gravity environment will be increased significantly.
- A low gravity environment would appear to offer a unique means of satisfactorily infiltrating a larger and/or complex shaped compact.

Approved:

N E Chatterton

N. E. Chatterton, Ph. D.
Manager
Research Laboratories

TABLE OF CONTENTS

TABLE OF CONTENTS - Concluded

LIST OF ILLUSTRATIONS

LIST OF ILLUSTRATIONS - Concluded

1. INTRODUCTION

The weightless conditions in an orbiting spacecraft offer some unique advantages for work on materials and processes that can yield valuable returns. One of the main advantages of this weightless condition foreseen for achieving such a result is the elimination of gravity-driven forces. This has been very clearly demonstrated through the low-gravity solidification of immiscibles (Ref. 1), where segregation effects due to density differences make bulk sample production practically impossible on Earth and in numerous other experiments (Ref. 2).

It appears that this unique condition can be very profitably utilized in material processes which simultaneously involve solid and liquid phases, such as liquid phase sintering (LPS). This is a processing technique where a mass of small particles of different components is heated above the melting temperature of one of the components so that all the particles become bonded into a solid mass on cooling. The two phases of this process may tend to separate due to density differences under the influence of gravity.

Sintering is a complex process consisting of a series of closely related physicochemical phenomena. It should be regarded as a thermodynamic process in which the system tends to attain a state with minimal free energy. In general, since the particle size of the solid phase is small and a liquid phase is involved, the mixture to be sintered becomes a capillary system. The behavior of such a system with highly developed surfaces, the distribution of phases within it, and consequently the properties of the body itself will depend to a considerable extent on the properties of the boundaries between the phases within the system. The field of forces acting on the dispersed particles in such a system

depends on the surface energies of the interphase boundaries. Hence, the kinetics of sintering and densification will also depend on the capillary properties of the system. It seems clear that certain minimum requirements regarding the wetting of the solid phase by the liquid during sintering must be met in order to successfully sinter with a liquid phase. In an otherwise non-wetting system, wetting can be achieved by decreasing the solid-liquid interfacial energy through preferential adsorption of one of the constituents in the liquid phase on the surface of the solid phase and/or by diffusion fluxes.

The necessary interface condition of wetting is effected by both gravity and the environment. It has been pointed out in a theoretical study (Ref. 3) that the adsorption of the residual gases of the space environment, which contain a high percentage of O and O_2, will affect the specific surface energy of both the solid and liquid phases. It was also shown that both vacancy concentration and thermal faceting are functions of surface energy.

The present study effort is concerned with forming of some LPS compacts using selected binary combinations of materials, studying their densification and microstructural properties, and developing an analytical model that will indicate the effect of gravity on LPS and also corroborate with the present experiments.

Also included in the study is a design and definition of a space experiment to prove the effects of gravity on the properties of LPS compacts. This has been developed based on the present analytical and experimental studies.

2. LIQUID PHASE SINTERING PROCESSES

2.1 GENERAL

During sintering, there are several separate mechanisms which can operate simultaneously to alter the microstructure of the material. Shaler (Ref. 4) has classified these into the "transient mechanisms" and the "steady-state phenomena".

The "transient mechanisms" are phenomena which are not, in general, absolutely necessary to sintering, but which can be made to occur by special treatment of the components of the compact. Such mechanisms as the desorbtion of absorbed or adsorbed gases and chemically absorbed surface compounds, surface atomic rearrangement (i.e., recrystallization), volume recrystallization and thermally relieved residual stresses, all of which tend to occur more during the first stages of sintering, are transient mechanisms.

The "steady-state phenomena" are changes that go on during sintering no matter how the powders are prepared and cannot be divorced from the sintering process. Such mechanisms as interparticle attractions, surface tension forces, gravity-driven buoyancy forces, and corresponding densification or swelling of the compact are examples of steady-state phenomena.

According to Shaler (Ref. 4), when the temperature of a metallic powder is slowly raised, the following transient events generally occur in order: 1) physcially adsorbed gases are desorbed; 2) there is an atomic rearrangement of the surface, a sort of two-dimensional surface recrystallization; 3) there is a breakdown of chemically adsorbed surface compounds; 4) and a recrystallization occurs in the volume of the metal. All of these changes are thought to be completed fairly rapidly at lower temperatures than those generally used in sintering (for a counter argument see the discussion of Ref. 4).

Among the steady-state phenomena, the attraction between particles, the spheroidization of voids, and associated densification or swelling of the compact can be distinguished.

As the plastic stage is reached, the mechanisms influencing the microstructure appear to become very interrelated, even to the point where such suggested separation as transient and steady state has been questioned. For example, as a result of pressing, the core of a compact is in compression while the outside surface is in tension. When the compact is heated, the surface residual stress is thermally relieved first, leading to an initial expansion. Shortly thereafter the material near the surface probably enters the plastic regime. In the plastic state, surface tension forces start to dominate, causing the movement of material in accordance with minimizing surface energies and producing shrinkage.

Overall, a significant degree of shrinkage of the material occurs prior to reaching the liquidus phase. Mackenzie and Shuttleworth (Ref. 5) cite experimental data in which a compact of tungsten powder heated to just below its melting point had all its linear dimensions decreased by approximately 17 percent in only 15 minutes.

As the liquidus/solidus phase is reached, two significant mechanisms exist which promote the movement of the solid particles. First, the intervening liquid in conjunction with the surrounding void space offers considerably less resistance to any movement of solid particles than it did as a solid. Second, if the liquid/solid have good wetting characteristics the liquid coats the solid in such a way that the resultant surface tension forces pull adjacent particles together. In the simplest possible terms, the surface tension force is inversely proportional to the effective radius of the surrounding void -- which

for compacts is very small -- causing the surface tension force to be relatively large. As the process continues the liquid tends to completely coat the solid particles. Pores are formed in the liquid phase and the decrease in the liquid/vapor pore surface area and consequently the overall surface energy becomes the driving force leading to densification. Within the pore there is a pressure given by

$$p_p = \frac{2\sigma_{\ell v}}{r_p} \qquad (2\text{-}1)$$

where

p_p - pore pressure

$\sigma_{\ell v}$ - liquid/vapor surface tension

r_p - pore radius.

Because of surface tension effects the pressure inside the pore is greater than the surrounding liquid hydrostatic pressure. As a result, an equivalent hydrostatic pressure is exerted on the entire liquid solid particle system which tends to rearrange particles to give maximum packing. The decrease in surface area of the pores and the interactions between the pores, the solids, and the liquid provides one of the main driving forces during sintering.

As opposed to the previous view of the sintering process, if the liquid/solid has poor wetting characteristics the liquid tends to spheroidalize. As a result, the pressure within the liquid would be greater than the surrounding hydrostatic pressure. The liquid pressure plus the resultant repulsive surface tension force component tends to separate the solid particles, causing the compact to swell.

Increased densification is one of the important properties of sintered materials. Lenel (Ref. 6), Gurland and Norton (Ref. 7),

and Kingery (Ref. 8), in studies of the phenomenological aspects of the sintering process, have agreed that the following three conditions tend to increase densification:

- An appreciable amount of liquid must be present.
- An appreciable solubility of the solid into the liquid must be possible.
- Good wetting of the liquid with respect to the solid must exist.

2.2 THE THEORY

The earlier theories of LPS were formulated by Price, Smithells, and Williams (Ref. 9) in a study of the sintered alloy of W-Ni-Cu system. The theory was subsequently developed by Lenel (Ref. 10), Gurland and Norton (Ref. 7), and Cannon and Lenel (Ref. 11), who proposed both heterogeneous and homogeneous processes, and suggested a three-stage sintering mechanism for the densification.

The densification process can be best understood by considering the forces acting on the system due to the surface energies involved. According to Lenel (Ref. 10), even with slight solubility of the solid component in the liquid phase, there is a constant interchange of atoms. The most mobile atoms on the edges and corners of the solid particles, having a large free-energy reserve, go into solution and are then reprecipitated in areas where the atoms are least mobile. When the liquid first melts, it tends to completely coat the solid particles. Pores are formed in the liquid phase and the decrease in the liquid-vapor pore surface area and consequently the overall surface energy is the driving force leading to densification through one or more of the three-stage mechanism. These three stages are discussed in the following subsections.

2.1.1 Rearrangement Process

On initial formation of liquid phase on melting, capillary pressure will tend to rearrange the solid particles in such a way as to give maximum packing and a minimum of resultant pore surface. This initially can take place by particles sliding over one another. Subsequently, bridges are built up which will collapse by the solution of a small amount of material at the contact points. When this takes place, substantial rearrangement of neighboring particles can take place with an ultimate arrangement of solid particles in a way consistent with high density. The rate of densification follows a relation

$$\frac{\Delta L}{L_0} = \frac{1}{3}\frac{\Delta V}{V_0} = Kt^{(1+y)} \qquad (2\text{-}2)$$

where

L_0, V_0 - initial length and volume

ΔL, ΔV - changes in length and volume

t - time

K - a constant of proportionality which depends on composition and temperature

y - a small fraction.

The volume of pores between the solid particles amounts to 25 to 50 percent, depending on the degree of packing and the particle size. For a volume of liquid phase material less than the minimum required for complete densification, the degree of densification decreases. In this case, other sintering processes are necessary for the complete densification (Figure 2-1).

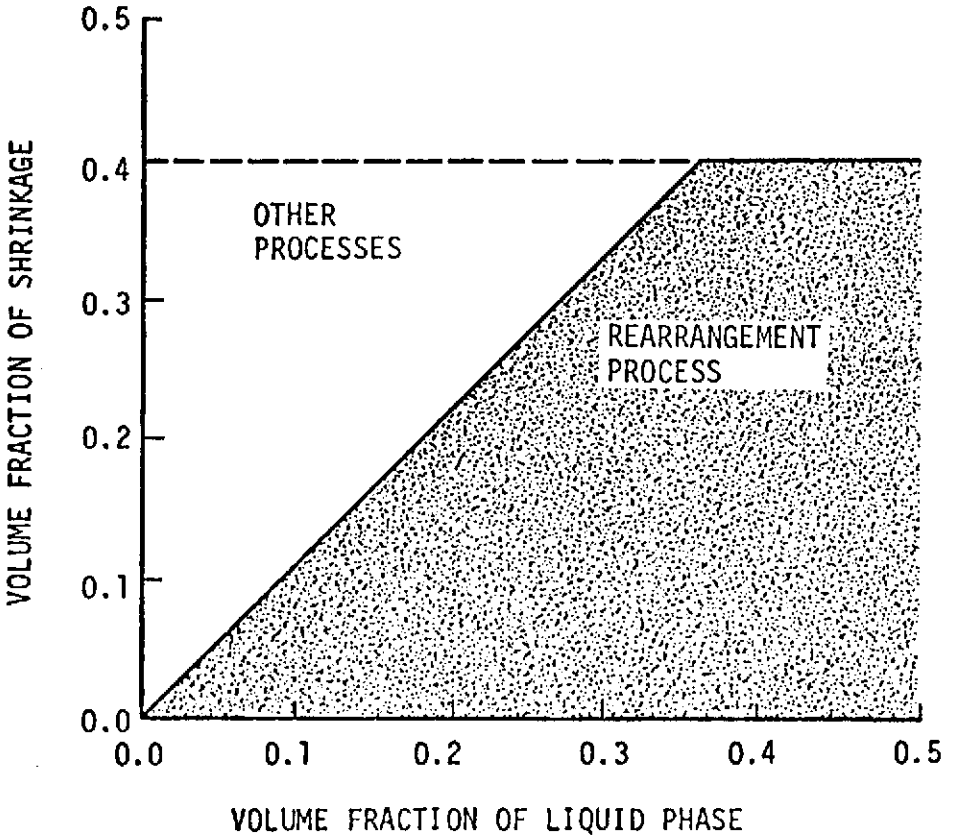

FIGURE 2-1. SHRINKAGE DUE TO THE "REARRANGEMENT" PROCESS WITH DIFFERENT LIQUID CONTENTS (INITIAL SPECIMEN POROSITY 40 PERCENT)

2.1.2 Solution-Reprecipitation Process

Once the rearrangement process has been completed, densely packed solid particles separated by thin-liquid films carry the major part of the compressive stress at the contact points. The solubility at the contact points between particles is larger than the solubility of other solid surfaces and this results in the transfer of material away from the contact points, allowing the center-to-center distance between particles to be decreased and densification to take place.

A condition for the occurrence of this process is the penetration of the liquid between the grains. The extent to which the liquid enters

the joints between the particles depends on the dihedral angle formed by the liquid phase at the boundary with two grains of the solid phase (Figure 2-2). Under equilibrium conditions, this angle can be expressed as

$$\sigma_{S_1-S_2} = 2\,\sigma_{S-L}\cos\phi/2 \qquad (2-3)$$

where

$\sigma_{S_1-S_2}$ - interfacial energy at the boundary between the two grains of the same phase

σ_{S-L} - interfacial energy at the boundary between the solid and liquid phases

ϕ - dihedral angle.

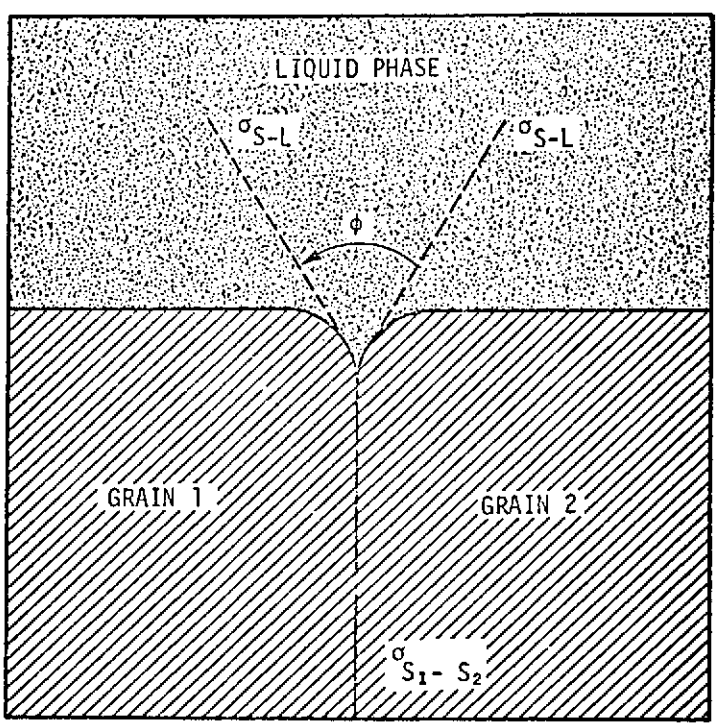

FIGURE 2-2. DIHEDRAL ANGLE FORMED BY LIQUID PHASE AT THE BOUNDARY OF TWO GRAINS OF SOLID PHASE

Analysis of the equation shows that for

$$\sigma_{S-L} > \frac{1}{2}\sigma_{S_1-S_2} \qquad 180° > \phi > 0$$

$$\sigma_{S-L} = \sigma_{S_1-S_2} \qquad \phi = 120°$$

$$\sigma_{S-L} < \frac{1}{2}\sigma_{S_1-S_2} \qquad \text{No value of } \phi \text{ satisfies equation.}$$

In studying the distribution of particles in heterogeneous systems, investigation of wettability and determination of angle of contact at the liquid/solid interface are performed.

2.1.3 Formation of Rigid Skeleton

In the third stage, the substance is slowly consolidated as the result of the solid particles growing together in accordance with the rules of solid phase sintering. The result is that a rigid skeleton is formed in the body undergoing sintering.

As shown above, the extent to which the liquid flows between the solid particles depends on the value of the dihedral angle. At a certain ratio between the surface energies at the solid/solid and solid/liquid boundaries, it may turn out that the liquid will not flow into the joints between the particles. This occurs when the interfacial tension does not satisfy the relationship

$$\sigma_{S_1-S_2} > 2\,\sigma_{S-L}\,. \qquad (2-4)$$

In this case, the neighboring particles of the solid phase may weld together. The greater the number of welded particles, the more difficult is the flow of the liquid. Sometimes the number of such bonds is so great that almost all particles of the solid phase grow together, creating their own skeleton, with the liquid phase enclosed in the pores.

3. LPS MODEL

3.1 FUNDAMENTAL CONCEPT

During various stages of the sintering process, a simple LPS can be viewed as a trinary system. Figure 3-1 shows schematically the microstructure of an LPS during the various stages of sintering. In the green state, after the work piece has been compacted, the individual particles, according to Goetzel (Ref. 12), are held together by interatomic forces (i.e., surface adhesion and cold welding) and mechanical interlocking. In this state the LPS compact is a solid/solid/void or, more correctly, a solid/solid/gas system. The void fraction depends on the plasticity of the base materials, the particle sizes and shapes, compacting pressure, and other factors. During the sintering process the compacted material goes from a solid/solid/gas to solid/liquid/gas, and back to a solid/solid/gas system.

Letting f_s, $f_{\ell s}$, f_v represent the volume fractions of the higher melting point solid, the lower melting point solid, and the void, respectively, it is obvious that for this simple LPS compact,

$$f_s + f_{\ell s} + f_v = 1. \tag{3-1}$$

Maximum densification of the final product occurs when $f_v \rightarrow 0$.

During the sintering process the void fraction changes from its initial value to some final value and the difference accounts for most of the shrinkage.

Packing of particles is a debatable point in any theoretical colloid or particle problem. Most of the theoretical LPS models depict the compact ideally as many spheres in contact. For this simple

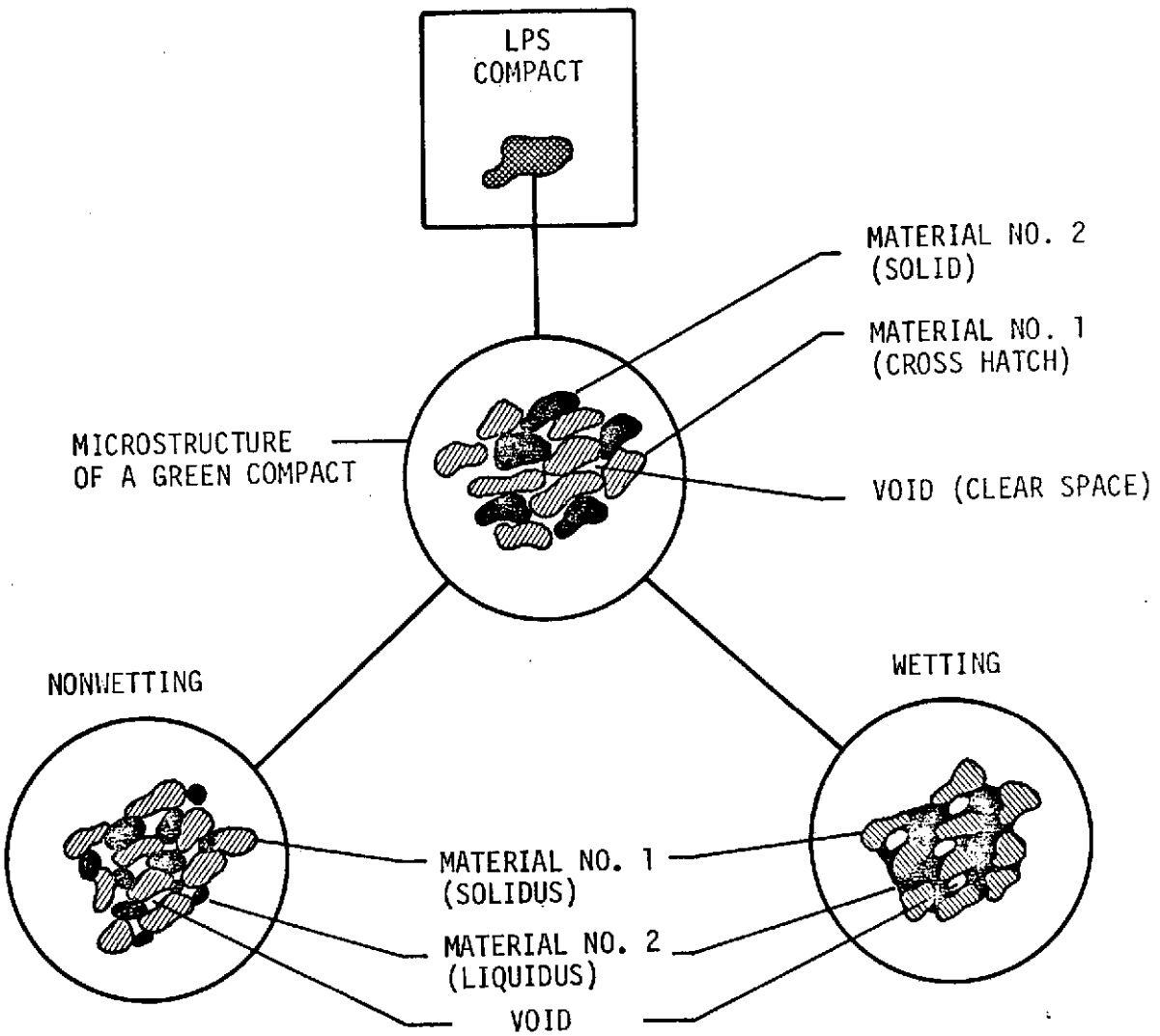

FIGURE 3-1. LPS MICROSTRUCTURE DURING VARIOUS PHASES OF SINTERING

problem the maximum and minimum pore space (i.e., void volume) can be derived by considering the gross volume occupied by each sphere. The maximum and minimum pore space occurs when the spherical packing is cubic and rhombohedral, respectively, as shown in Figure 3-2. The gross volume occupied by each sphere is the volume of an imaginary container constructed by passing tangent planes through the nearest points of contact of the spheres. As can be seen in Figure 3-2, for cubic packing, each central sphere has six neighbors and the resulting figure is a cube. For rhombohedral packing, each central sphere has 12 neighbors, resulting in a rhombic dodecahedron container. Obviously the void volume associated with each sphere will be the volume of the container minus the volume of the sphere. Assuming the spheres to be uniformly spaced a distance ℓ apart and letting R be the radius of the sphere, the total volume occupied by each sphere and its pore space (i.e., the volume of the imaginary container) is,

cubic packing
$$V_t = 8\left(R + \frac{\ell}{2}\right)^3 \tag{3-2}$$

rhombohedral packing
$$V_t = \frac{8}{\sqrt{2}}\left(R + \frac{\ell}{2}\right)^3 \tag{3-3}$$

where V_t is the total volume.

Letting the spheres represent solid particles of an LPS, it can be seen that the volume fraction of solid (f_s) is given as

$$f_s = \frac{V_s}{V_t} \tag{3-4}$$

where V_s is the volume of a sphere (i.e., the solid particle being depicted as a sphere). During sintering, the theoretical model is depicted as many spheres connected by small amounts of liquid, as

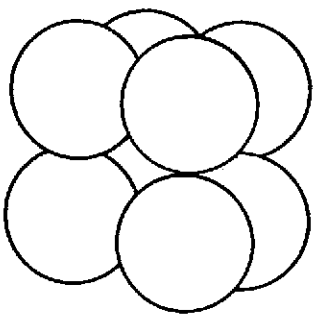

CUBIC PACKING

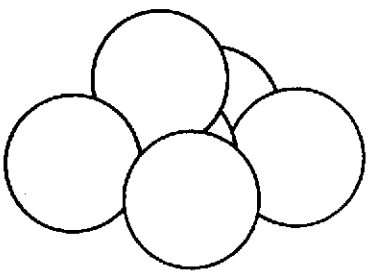

RHOMBOHEDRAL PACKING

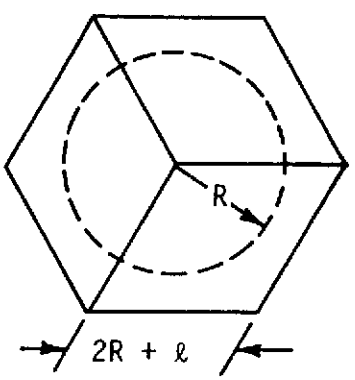

CUBE

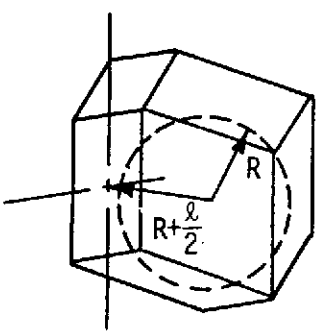

RHOMBIC DODECAHEDRON

FIGURE 3-2. CUBIC AND RHOMBOHEDRAL PACKING

shown in Figure 3-3. For this condition the volume surrounding the solid is occupied partially by the liquid and partially by the void. The liquid volume can be defined as

$$V_\ell = n v_\ell = V_t f_{\ell s} \tag{3-5}$$

where

V_ℓ - total liquid volume associated with each sphere

n - number of spheres surrounding each central sphere (i.e., n = 6 for a cube and n = 12 for a rhombic dodecahedron)

v_ℓ - the liquid volume associated with each contact

$f_{\ell s}$ - liquid volume fraction.

If the liquid volume is known or can be deduced for a given condition, then Equation 3-1 gives

$$f_v = 1 - (f_s + f_{\ell v}) = 1 - \frac{V_s + V_\ell}{V_t}$$

$$= 1 - \frac{V_s + n v_\ell}{V_t} \quad . \tag{3-6}$$

From Equations 3-4, 3-5, and 3-6 it is possible to compute the volume fractions of any of the components, which gives for cubic packing

$$(f_s)_{cp} = \frac{\pi}{6} \cdot \frac{R^3}{(R + \ell/2)^3} \tag{3-7a}$$

$$(f_{\ell s})_{cp} = \frac{2/3\ V_\ell}{(R + \ell/2)^3} \tag{3-7b}$$

$$(f_v)_{cp} = 1 - \frac{4/3\ \pi R^3 + 6\ V_\ell}{8(R + \ell/2)^3} \quad . \tag{3-7c}$$

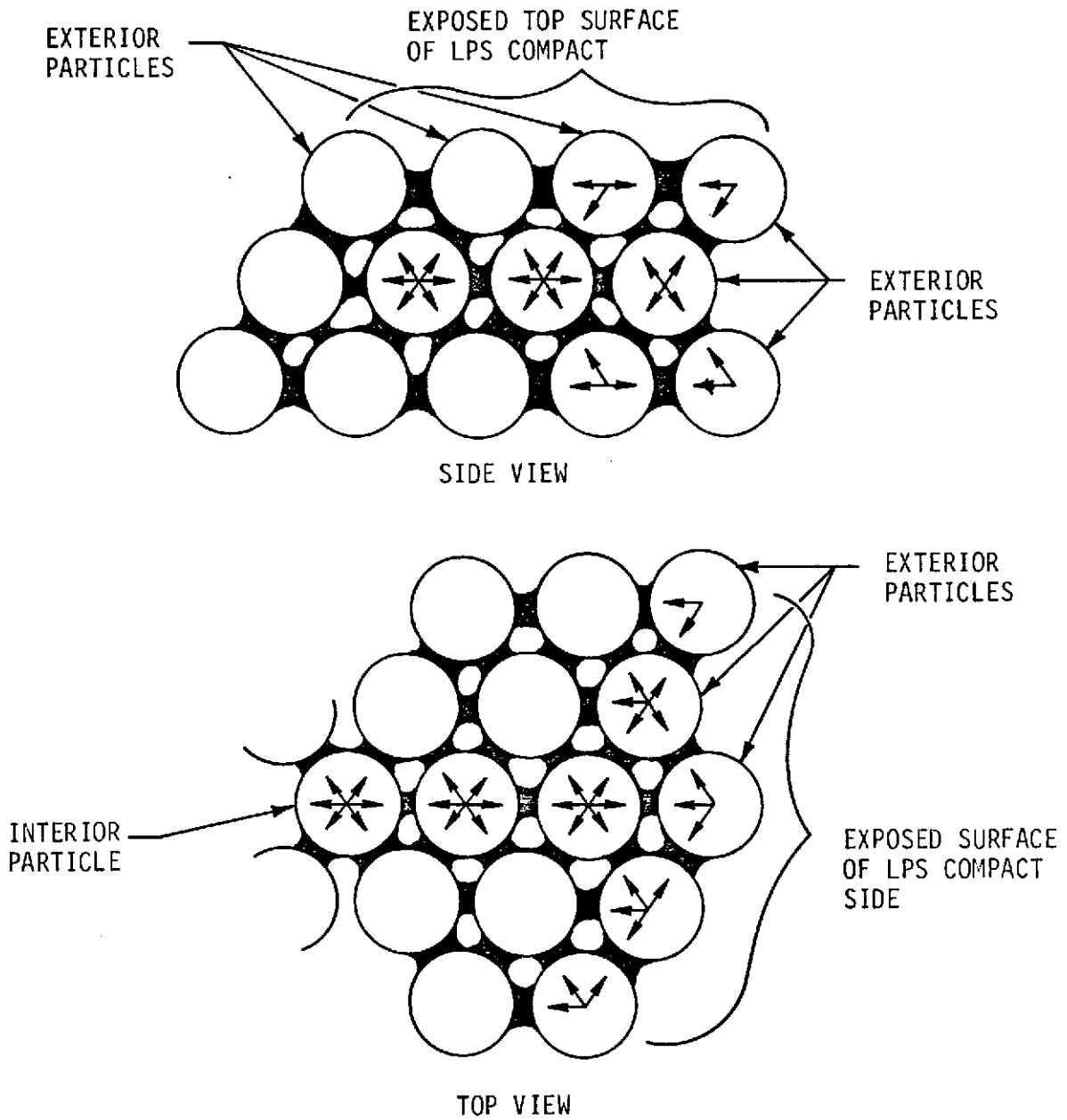

FIGURE 3-3. SOLID/LIQUID MODEL

and for rhombohedral packing,

$$(f_s)_{rp} = \frac{\sqrt{2}\,\pi}{6} \frac{R^3}{(R + \ell/2)^3} \tag{3-8a}$$

$$(f_{\ell s})_{rp} = \frac{\sqrt{2}}{8} \frac{12\ V_\ell}{(R + \ell/2)^3} \tag{3-8b}$$

$$(f_v)_{rp} = 1 - \frac{\sqrt{2}\ (4/3\ \pi\ R^3 + 12\ V_\ell)}{8(R + \ell/2)^3} \quad . \tag{3-8c}$$

For close packing, i.e., $\ell = 0$ and for no liquid, Equations 3-7c and 3-8c give maximum and minimum void fractions of

$$(f_v)_{cp} = 0.4764$$

and

$$(f_v)_{rp} = 0.2595.$$

These void fractions are very nearly the same as those found experimentally to vary from $0.25 \leqq f_v \leqq 0.5$.

3.2 MODELING OF SURFACE TENSION FORCES

Depicting the compact ideally as many spheres, with adjacent spheres connected at their nearest points by a small amount of liquid (see Figure 3-3), can explain some of the forces acting during the sintering process. Adjacent spheres are attracted or repelled because of the capillary-like forces which are produced by the intervening liquid. For a wetting liquid the forces are attractive; therefore, an interior particle, as depicted in Figure 3-3, is subject to attraction in all directions by neighboring particles. Particles on the surfaces

are attracted inward and to the sides by neighboring particles, but there is no outward attraction to balance the inward pull. Hence, every surface particle is subject to inward attraction more or less perpendicular to the surface. For conditions where no other forces act to prevent inward movement, the exterior particles tend to move inward, causing omnidirectional shrinkage. It is possible to model the capillary forces by considering two spheres with an intervening liquid as shown in Figure 3-4. In the general case the liquid-vapor interface shape varies as depicted in Figure 3-4. Because of hydrostatic forces, the radii of curvature are assumed to vary with the angles α and β. Later it will be shown that constant radii of curvature is a very safe assumption for LPS.

For a wetting liquid the pressure (P_ℓ) on the liquid side of the liquid-vapor interface is less than the pressure (P_v) on the vapor side. Therefore, the spheres are subjected to a compressive force given by

$$dF_1 = (P_v - P_\ell)\, dA_{\alpha, z} \tag{3-9}$$

where

dF_1 - hydrostatic force acting to attract the spheres (note that when $dF_1 < 0$, the force is repulsive)

$dA_{\alpha, z}$ - projection of the wetted area on the α, z plane.

A surface tension component opposite to the σ vector shown in Figure 3-4 is also acting to pull the spheres together. A differential surface tension force is given by

$$dF_2 = \sigma_{\ell v} \cos [\, 90 - (\phi_0 + \theta)\,]\, dS \tag{3-10}$$

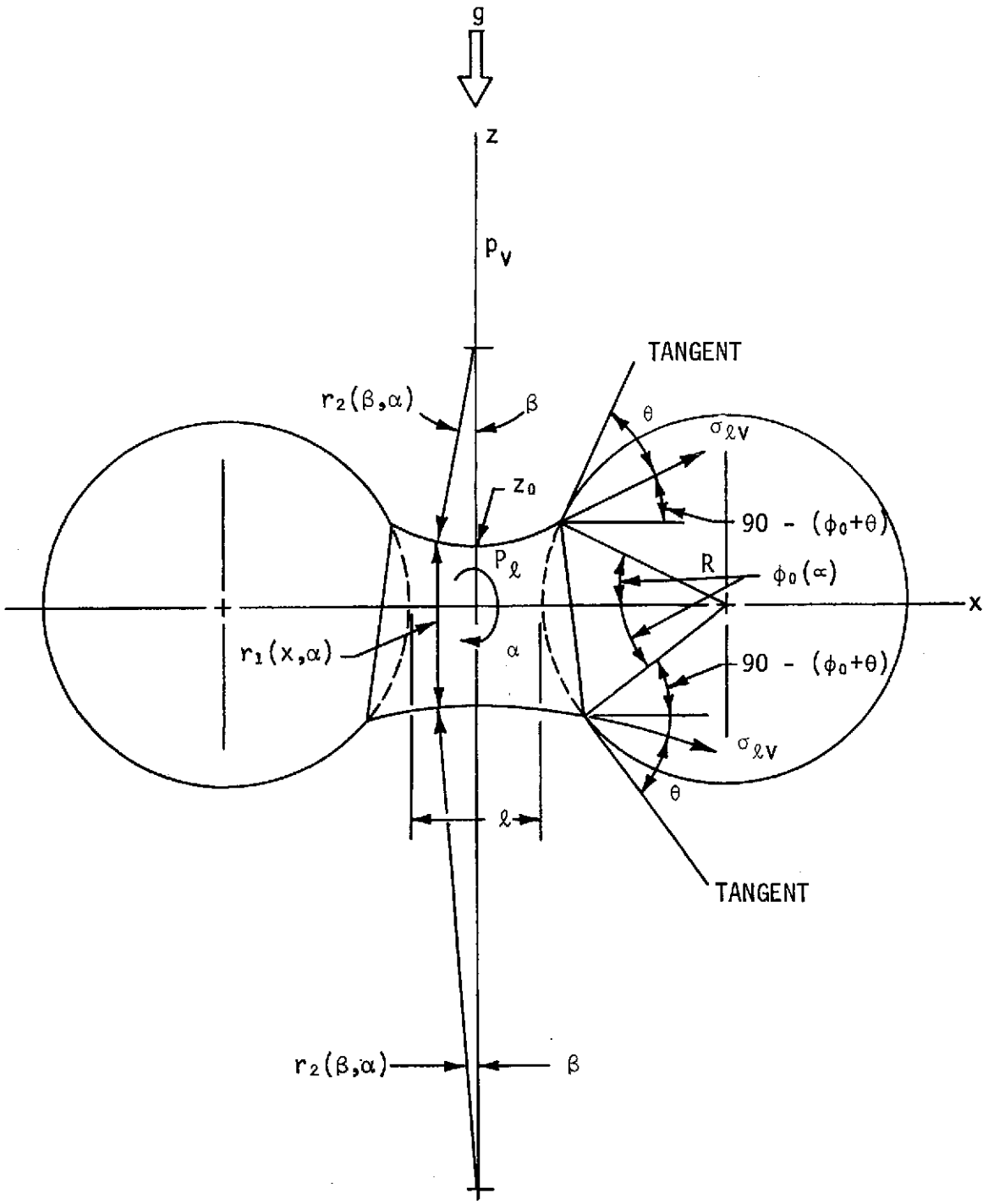

FIGURE 3-4. TWO-SPHERE SURFACE TENSION MODEL

where

dF_2 - surface tension force acting to attract the spheres (note that when $dF_2 < 0$, the surface tension force is repulsive)

$\sigma_{\ell v}$ - liquid-vapor surface tension

dS - liquid-solid wetted perimeter increment

ϕ_0 - angle between the sphere centerlines and the wetted perimeter

θ - liquid, solid contact angle.

Letting

$$dA_{\alpha, z} = R \sin\phi \, d\alpha \cdot d(R \sin\phi) \tag{3-11}$$

$$dS = R \sin\phi \, d\alpha \ . \tag{3-12}$$

Then the resultant force is given by

$$\begin{aligned} dF &= dF_1 + dF_2 \\ &= (P_v - P_\ell) R \sin\phi \, d(R \sin\phi) \, d\alpha \\ &\quad + \sigma_{\ell v} \sin(\phi_0 + \theta) R \sin\phi_0 \, d\alpha \ . \end{aligned} \tag{3-13}$$

The integration of Equation 3-13 requires a complete definition of the interface shape and the hydrostatic forces. The hydrostatic forces can be related to the surface tension through Laplace's first law, giving

$$P_v - P_\ell = \sigma_{\ell v} \left(\frac{1}{r_2} - \frac{1}{r_1} \right) \tag{3-14}$$

where r_1 and r_2 are the principal radii of curvature at any point on the liquid-vapor surface (α, x, z). Assuming an acceleration vector (g) to be aligned with the z axis the hydrostatic pressure on the liquid side of the liquid-vapor interface is given by

$$P_\ell = P_{\ell o} + \rho_\ell \left(\frac{g}{g_0}\right) (z_0 - z) \tag{3-15}$$

where

$P_{\ell o}$ - hydrostatic pressure at the interface where $\alpha = 0$, $x = 0$, $z = z_0 = r_{1\,0}$ (i.e., top, center of the interface)

ρ_ℓ - liquid density

g_0 - sea level gravitational constant.

Since $z = r_1 \cos \alpha$, Equation 3-15 can be written as

$$P_\ell = P_{\ell o} + \rho_\ell \left(\frac{g}{g_0}\right) (r_{10} - r_1 \cos \alpha) \ . \tag{3-16}$$

Then, Equation 3-14 becomes

$$(P_v - P_\ell) = P_v - P_{\ell o} - \rho_\ell \left(\frac{g}{g_0}\right) (r_{10} - r_1 \cos \alpha)$$

$$= \sigma_{\ell v} \left(\frac{1}{r_2} - \frac{1}{r_1}\right) \ . \tag{3-17}$$

At the point $\alpha = 0$, $x = 0$, $z = z_0$, Equation 3-14 gives

$$P_v - P_{\ell o} = \sigma_{\ell v} \left(\frac{1}{r_{20}} - \frac{1}{r_{10}}\right) \ . \tag{3-18}$$

Then, defining a mean radius of curvature as

$$\frac{2}{r_m} = \left(\frac{1}{r_2} - \frac{1}{r_1}\right) \tag{3-19}$$

and

$$\frac{2}{r_{mo}} = \left(\frac{1}{r_{20}} - \frac{1}{r_{10}}\right) \tag{3-20}$$

Equation 3-17 gives

$$\frac{(P_v - P_\ell)}{\sigma_{\ell v}} = \frac{2}{r_{mo}} - \frac{\rho_\ell}{\sigma_{\ell v}}\left(\frac{g}{g_0}\right)(r_{10} - r_1 \cos\alpha) = \frac{2}{r_m} \quad . \tag{3-21}$$

Equation 3-21 can be rearranged to give

$$\frac{r_{mo}}{\sigma_{\ell v}} (P_v - P_\ell) = 2 - B_o\left(\frac{r_{10} - r_1 \cos\alpha}{r_{mo}}\right) \tag{3-22}$$

where B_o is the Bond number given by

$$B_o = \frac{\rho_\ell (g/g_0) r_{mo}^2}{\sigma_{\ell v}} \quad . \tag{3-23}$$

From Equation 3-22, the simple relation obtained is

$$\frac{r_{mo}}{r_m} = 1 - \frac{1}{2} B_o\left(\frac{r_{10} - r_1 \cos\alpha}{r_{mo}}\right) \quad . \tag{3-24}$$

Equation 3-24 can be viewed as a measure of the eccentricity of the vapor-liquid interface. Table 3-1 lists the density and surface tension of several common LPS liquid phase materials in addition to those of water.

TABLE 3-1. LPS LIQUID PROPERTIES

MATERIAL	SP. GR.	$\sigma_{\ell v}$ (dyne/cm)	$\rho/\sigma_{\ell v}$ [gm/(dyne cm^2)]
Cu	8.9	1270	0.007
Ag	10.5	940	0.01117
Pb	11.3	455	0.02484
CaO	3.3	820	0.00402
MgO	3.6	1090	0.0033
H_2O	1.0	75	0.01333

Letting the mean radius of curvature r_{mo} in Equation 3-23 be equal to the radius of the sphere of Figure 3-4, the effects of gravity, particle radius, and the liquid density-surface tension ratio can be evaluated. From Table 3-1, it is seen that most of the common LPS liquids have density-to-surface-tension ratios of the order of $0.001 < (\rho / \sigma_{\ell v}) < 0.01$. For particle sizes ranging from 10 μ to 1,000 μ, the Bond numbers for various (g/g_0) levels have been computed and are shown in Figure 3-5. In most liquid phase sintering, particle sizes of the order of 10 μ to 100 μ are generally used. From Figure 3-5 it is seen that the Bond number for a one (g/g_0) environment is on the order of 10^{-3} and less. For the same size particles in a 10^{-4} (g/g_0) environment, the Bond number is 10^{-7} and less. Therefore, because the particle sizes in LPS are so small, the Bond number is significantly less than unity.

An understanding of how the Bond number affects the liquid-vapor interface shape can be obtained by considering the results derived by Hastings (Ref. 13). Using the principle of minimum energy, Hastings computed the liquid-vapor interface shape of a liquid confined in an axis-symmetric container as a function of Bond number. Dimensionless interface shapes for Bond numbers varying between 0 and ∞ are shown in Figure 3-6. Normally, in low-gravity fluid mechanics problems, the Bond number changes from a large number under one-g conditions to a very small number as gravity approaches zero. For example, a one-foot-diameter container of water has a Bond number of approximately $B_o = 3,000$ at one g, which reduces to $B_o = 0.3$ at $g/g_0 = 10^{-4}$. As can be seen in Figure 3-6, this causes the interface to change from a flat shape at one g to a nearly spherical shape at 10^{-4} g/g_0.

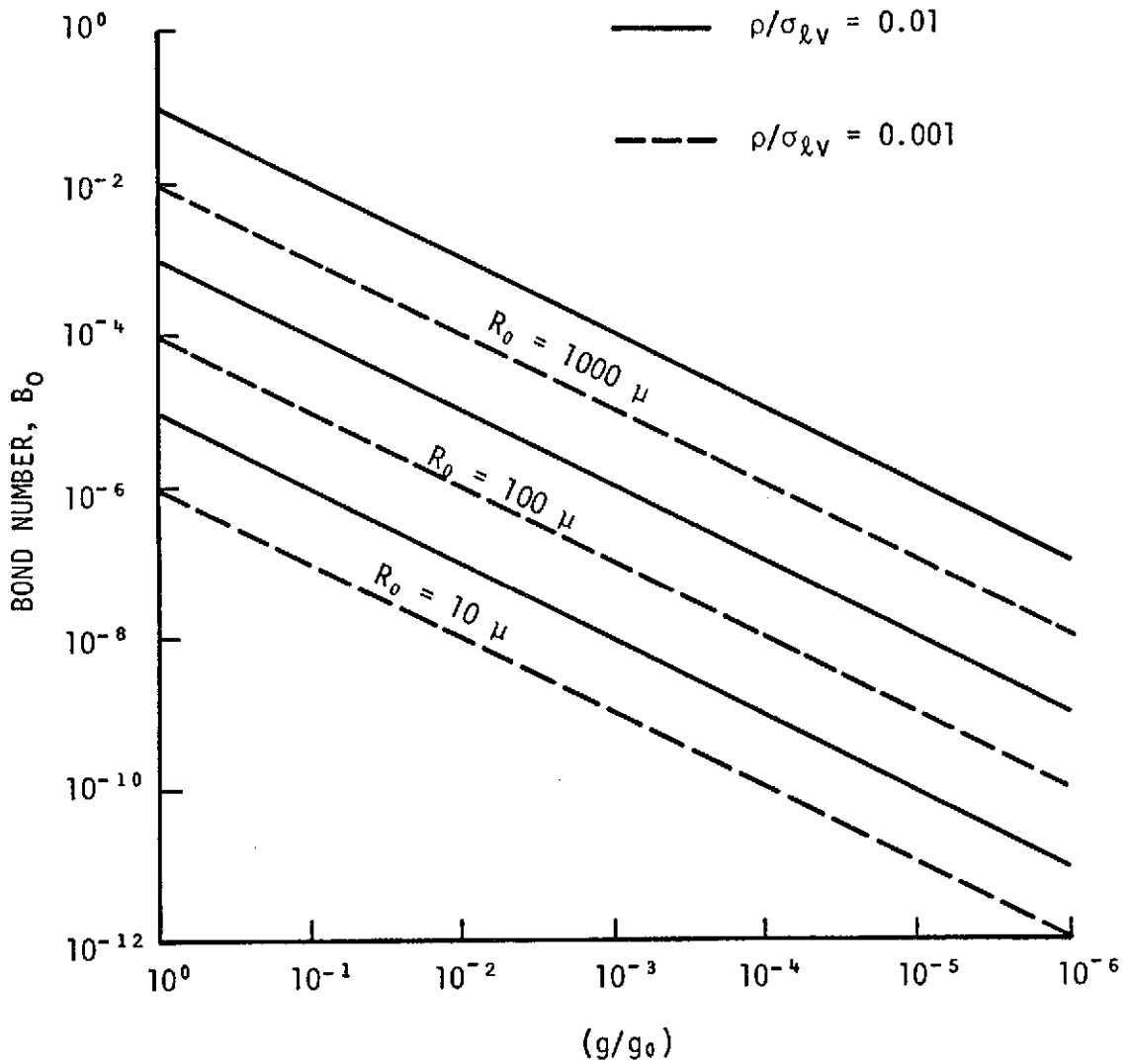

FIGURE 3-5. BOND NUMBER AS A FUNCTION OF GRAVITY FOR VARIOUS PARTICLE SIZES

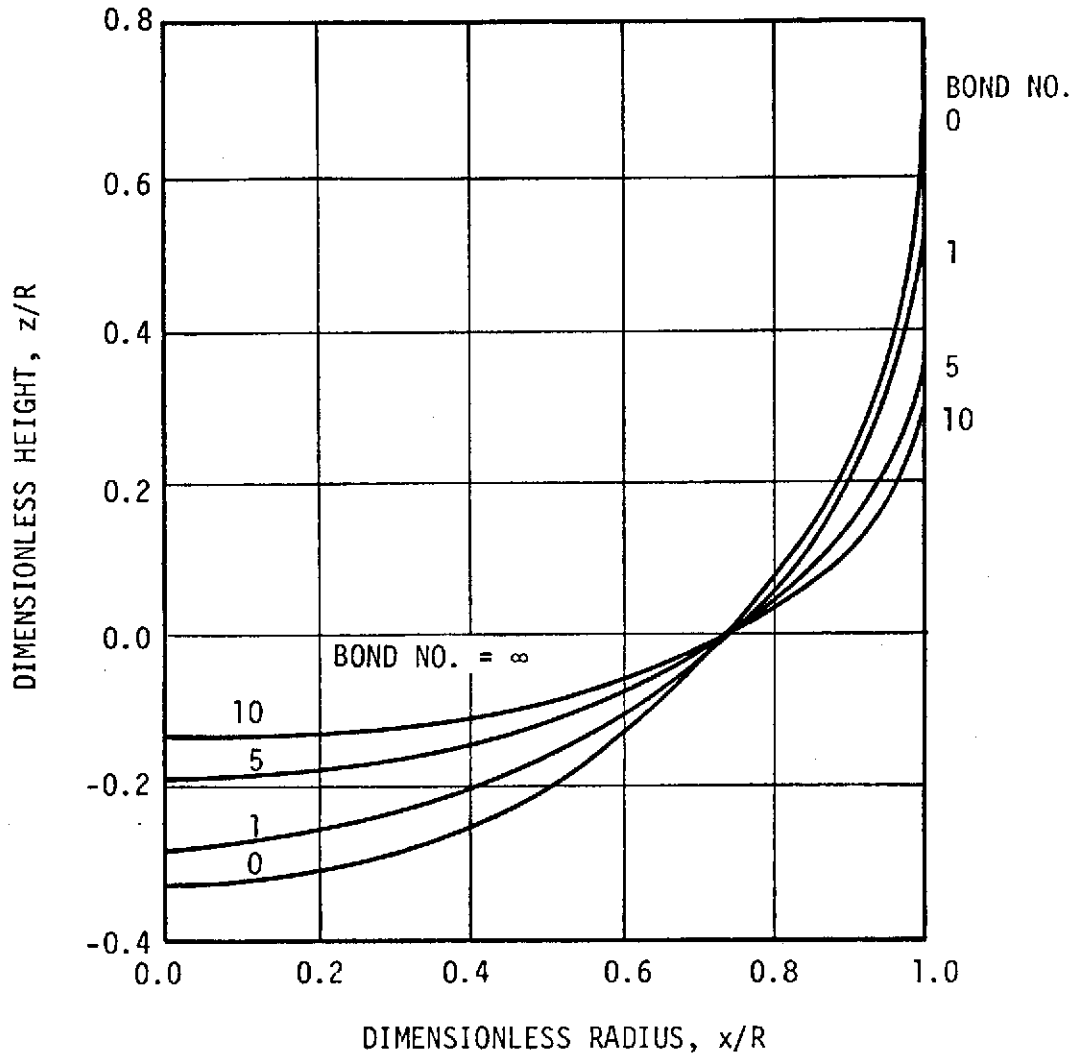

FIGURE 3-6. LOW-GRAVITY ZERO CONTACT ANGLE INTERFACE SHAPES IN CYLINDRICAL CONTAINERS

In liquid phase sintering, however, the particle sizes are so small that the Bond number is nearly zero even under one-g conditions. Reducing the Bond number further by reducing the gravitational component has a negligible effect on the interface shape. Therefore, Equation 3-24 gives

$$\lim_{B_o \to 0} \left(\frac{r_{mo}}{r_m} \right) = 1 \quad . \tag{3-25}$$

Thus, it is seen that as the Bond number tends to zero for whatever cause, the mean radius of curvature becomes a constant with respect to the variables α and β (see Figure 3-4). Equations 3-19 and 3-20 then give

$$\frac{2}{r_m} = \frac{2}{r_{mo}} = \left(\frac{1}{r_2} - \frac{1}{r_1} \right) = \left(\frac{1}{r_{20}} - \frac{1}{r_{10}} \right) \tag{3-26}$$

$$= \text{constant} \quad .$$

Equation 3-17 then gives

$$(P_v - P_\ell) = \frac{2\,\sigma_{\ell v}}{r_{mo}} \quad . \tag{3-27}$$

Equation 3-13 can then be written as

$$dF = \frac{2\,\sigma_{\ell v}}{r_{mo}} \, R \sin\phi \; d(R \sin\phi) \; d\alpha$$

$$+ \sigma_{\ell v} \sin(\phi_0 + \theta) \, R \sin\phi_0 \; d\alpha \quad . \tag{3-28}$$

Then since $r_m = r_{mo} = \text{constant}$, and ϕ is not a function of α for $[(1/r_{20}) - (1/r_{10})] = \text{constant}$, Equation 3-28 can be integrated to give

$$F = \int_0^{R \sin \phi_0} \int_{\alpha=0}^{2\pi} \frac{2 \sigma_{\ell v}}{r_{mo}} R \sin \phi \, d(R \sin \phi) \, d\alpha$$

$$+ \int_{\alpha=0}^{2\pi} \sigma_{\ell v} \sin (\phi_0 + \theta) R \sin \phi_0 \, d\alpha \qquad (3\text{-}29)$$

$$F = (2\pi) \left(\frac{\sigma_{\ell v}}{r_{mo}} \right) \frac{(R \sin \phi)^2}{2}$$

$$+ 2\pi \sigma_{\ell v} \sin (\phi_0 + \theta) R \sin \phi_0 \qquad (3\text{-}30)$$

or

$$F = \sigma_{\ell v} \left[\pi R^2 \sin^2 \phi_0 \left(\frac{1}{r_{20}} - \frac{1}{r_{10}} \right) + 2\pi R \sin \phi_0 \sin (\phi_0 + \theta) \right]. \qquad (3\text{-}31)$$

Letting ℓ be the distance between spheres gives

$$r_{10} = R \sin \phi_0 - \left[R(1 - \cos \phi_0) + \frac{\ell}{2} \right] \frac{1 - \sin (\phi + \theta)}{\cos (\phi + \theta)} \qquad (3\text{-}32)$$

$$r_{20} = \frac{R(1 - \cos \phi) + \frac{\ell}{2}}{\cos (\phi + \theta)} \qquad (3\text{-}33)$$

Naidich, et al (Ref. 14) studied the same problem, except that gravitational effects were ignored. Their derivation produced equations identical to Equations 3-31, 3-32, and 3-33.

Figures 3-7, 3-8, and 3-9 show how the surface-tension-induced, adhesive forces vary with the contact angle, distance between particles, and liquid fraction.

From Figure 3-7, it can be seen that the cohesive force decreases as the contact angle increases. The force is also seen to decrease as

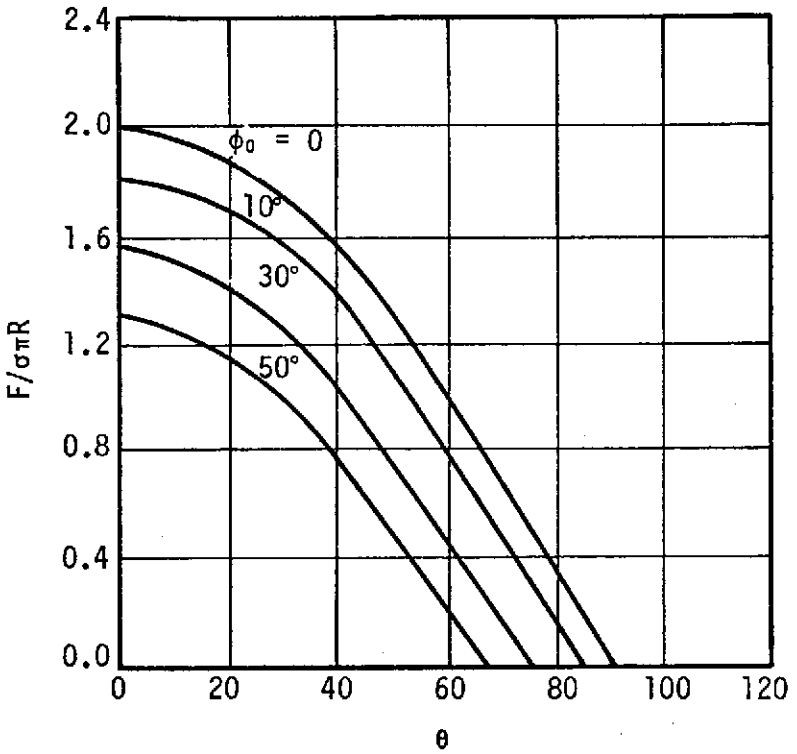

FIGURE 3-7. VARIATION OF COHESIVE FORCE WITH CONTACT ANGLE AND AMOUNT OF LIQUID PHASE

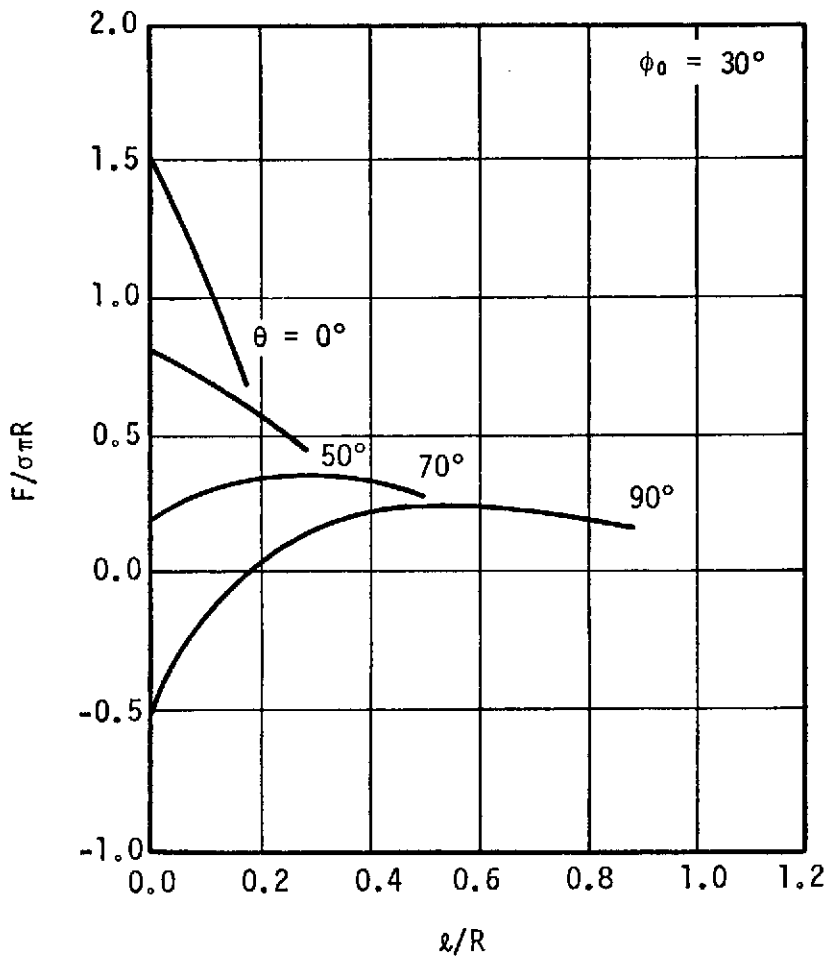

FIGURE 3-8. VARIATION OF COHESIVE FORCE WITH DISTANCE BETWEEN SPHERES FOR VARIOUS CONTACT ANGLES

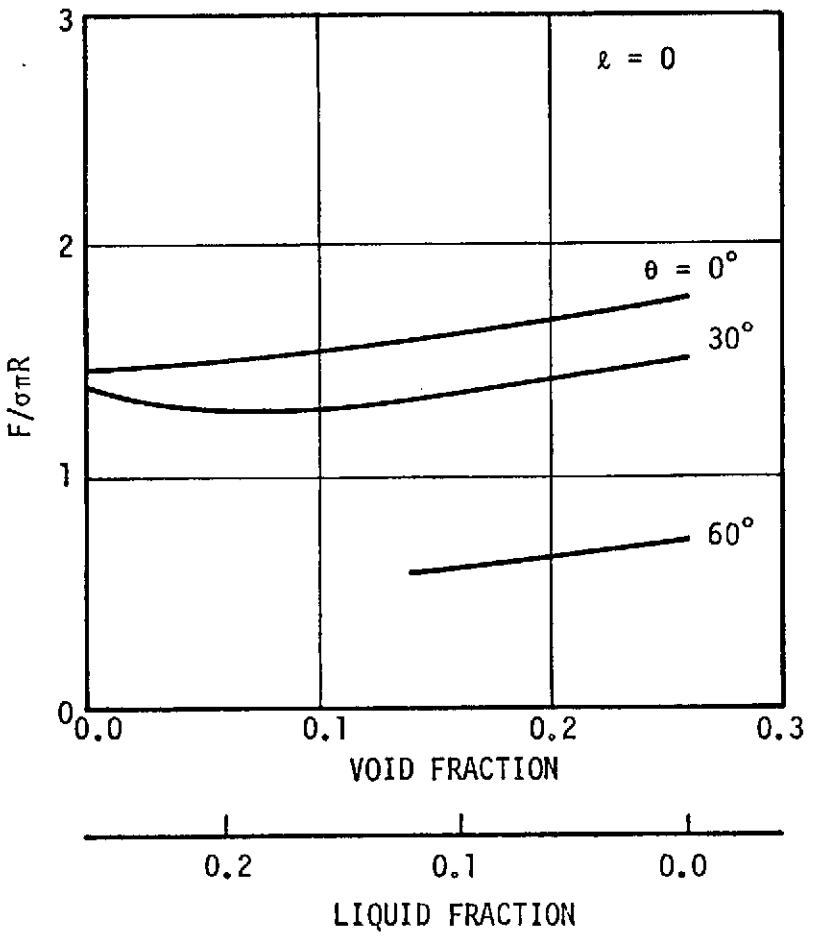

FIGURE 3-9. VARIATION OF COHESIVE FORCE WITH VOID FRACTION FOR DIFFERENT CONTACT ANGLES

the angle ϕ_0 increases (i.e., as more liquid is added). For any contact angle less than 90 degrees, it can be seen that the force becomes repulsive as the angle ϕ_0 is increased from the critical value where the force is zero.

Figure 3-8 shows how the cohesive force varies with distance between particles for $\phi_0 = 30°$. For highly wetting liquids (i.e., for θ near zero) the force is highest when the particles are touching and decreases as the distance between particles increases. For liquids where the contact angle approaches 90 degrees, the force is reduced as the distance between particles decreases. For $75° < \theta < 90°$ the forces are repulsive for distances between particles of $\ell/R < 0.2$. Referring to Figure 3-7 it is seen that as ϕ_0 increases, the contact angle at which the forces become repulsive decreases. This suggests a tendency of the particles to trap bubbles as shrinkage occurs.

Figure 3-9 shows how the cohesive force varies as the contact angle and liquid fraction are varied for the idealized rhombohedral packing with $\ell = 0$. This figure shows that the cohesive force varies only slightly as more liquid is added but decreases significantly as the contact angle is increased.

These results suggest that conditions can exist which cause the particles to tend to trap bubbles. This tendency is somewhat supported by the studies of liquid between cylinders carried out by Princen (Ref. 15). One of Princen's conclusions is shown schematically in Figure 3-10. As seen in Figure 3-10, when cylinders are moved together the entrapped liquid tends to separate into columns, leaving a void in the center. As the distance between cylinders was again increased, the void tended to spheroidalize and become entrapped.

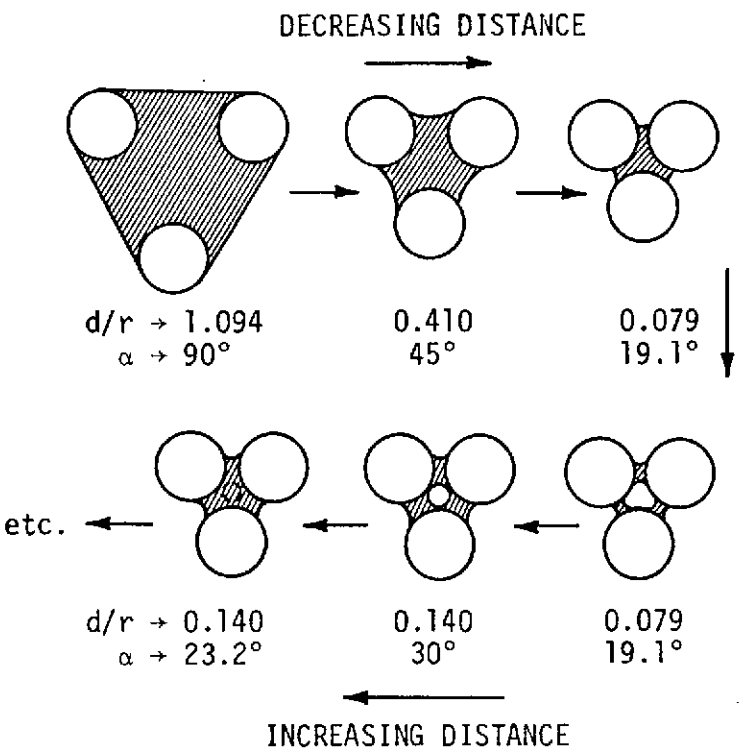

FIGURE 3-10. CYLINDERS WITH ENTRAPPED LIQUID

From the foregoing analysis and discussion it is concluded that a low-gravity environment will have only minor effects on the surface tension forces tending to pull particles together.

3.3 MODELING OF BUOYANCY FORCES

From the studies of Lenel (Ref. 6), Kingery (Ref. 8), Shaler (Ref. 4) and Machenzie and Shuttleworth (Ref. 5) it appears that during the sintering process voids turn into bubbles because of the tendency of surface tension forces to spheroidalize the voids. The bubbles appear to be formed uniformly throughout the compact and remain more-or-less locked in their original location. From these observations it would appear that the buoyancy forces are not sufficient to drive the bubble to a surface. However, it is known that segregation of material according to density shown schmatically in Figure 3-11 can occur, particularly whenever there is more liquid than that required to just fill the voids. The buoyancy forces acting on a particle (or a bubble in the case where bubbles tend to move) can be derived by considering the usual fluid mechanics of such a problem. Using Newton's second law it can be shown that a low-gravity environment would have a significant effect on slowing the settling process during liquid phase sintering.

Considering the forces acting on a particle settling as a result of gravity Newton's second law would give

$$F = ma = m\left(\frac{du}{d\tau}\right) \tag{3-34}$$

where

F - summation of all forces acting on the particle

m - mass of the particle

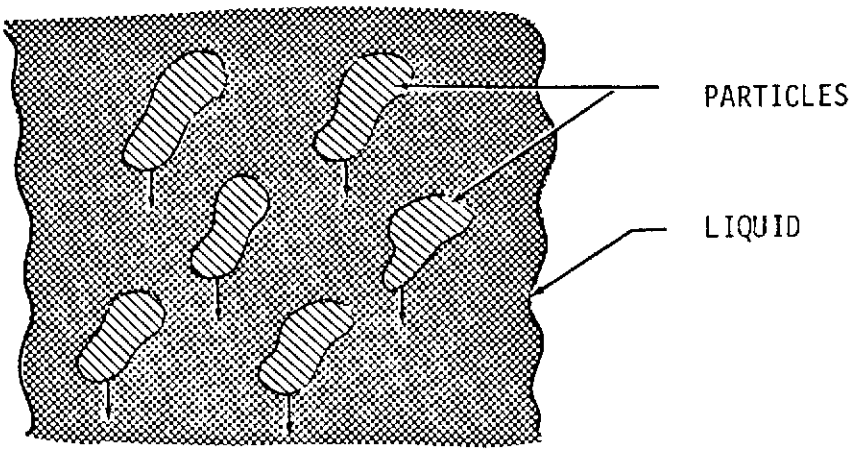

a. Particle Segregation

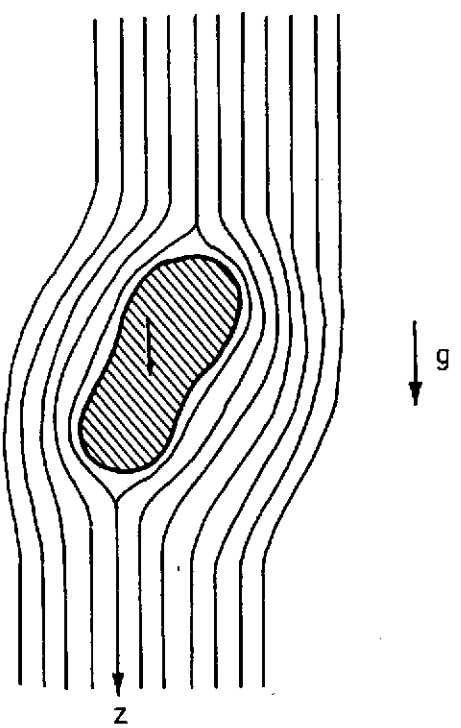

b. Particle Settling in a Liquid

FIGURE 3-11. PARTICLE SEGREGATION MODEL

u - velocity of the particle

τ - time.

Since the forces acting on the particle are buoyancy and drag, Equation 3-34 can be written

$$\frac{du}{d\tau} = g \frac{(\rho_\ell - \rho_s) V_s}{m} - \frac{C_D \frac{1}{2} \rho_\ell u^2 A_{cs}}{m}$$

$$\frac{du}{d\tau} = g \frac{(\rho_\ell - \rho_s) V_s}{\rho_s V_s} - \frac{C_D \frac{1}{2} \rho_\ell u^2 A_{cs}}{\rho_s V_s} \qquad (3\text{-}35)$$

where

ρ_ℓ - density of the liquid

ρ_s - density of the solid

V - volume of the solid

g - local gravitational force

C_D - drag coefficient

A_{cs} - representative cross sectional area corresponding to the drag coefficient C_D.

If it is assumed that the particle movement takes place at a constant velocity, then $du/d\tau = 0$ and Equation 3-35 gives

$$C_D u^2 = \frac{2g (\rho_\ell - \rho_s) V_s}{\rho_\ell A_{cs}} \qquad (3\text{-}36)$$

In most fluid flow problems, the drag coefficient can be very satisfactorily defined over a wide range by an empirical equation of the form

$$C_D = C N_{re}^{m} \qquad (3\text{-}37)$$

where

C, m - empirical coefficients

$N_{re} = \dfrac{\rho_\ell \, u \, D_s}{\mu_\ell}$ - Reynolds number

D_s - characteristic dimension

μ_ℓ - dynamic viscosity.

Substitution of Equation 3-37 into Equation 3-35 gives

$$u = \left[\frac{2 \, g \, V_s}{C \, A_{cs} \left(\dfrac{\rho_\ell \, D_s}{\mu_\ell} \right)} \cdot \left(\frac{\rho_\ell - \rho_s}{\rho_\ell} \right) \right]^{\frac{1}{2+m}} = \frac{dz}{d\tau} \qquad (3\text{-}38)$$

where z is the coordinate aligned with the direction of the gravitational force.

With the boundary conditions

$$z = z_i, \quad \tau = 0$$
$$z = z, \quad \tau = \tau$$

Equation 3-38 can be integrated to give,

$$\tau = (z - z_i) \left[\frac{2 \, g \, V_s}{C \, A_{cs} \left(\dfrac{\rho_\ell \, D_s}{\mu_\ell} \right)} \cdot \left(\frac{\rho_\ell - \rho_s}{\rho_\ell} \right) \right]^{-\frac{1}{2+m}} . \qquad (3\text{-}39)$$

Equation 3-39 gives the time required for a particle acted on by buoyancy and counteracted by body drag to move a distance $(z - z_i)$. If it is assumed that the coefficients C and m and the physical properties do not vary significantly in going from a one-g environment to a low-g environment, then the ratio of times required to move a given distance is given by Equation 3-39 directly as

$$\frac{\tau}{\tau_0} = \left(\frac{g_0}{g}\right)^{\frac{1}{2+m}} . \qquad (3\text{-}40)$$

Gorring and Katz (Ref. 16) have shown in studies of bubbles rising in clear liquids and in packed beds that the drag coefficients can be represented by Equation 3-37 over wide ranges in Reynolds numbers. Their results also show that the empirical exponent in Equation 3-37 is approximately $m \sim -1.0$. Thus Equation 3-40 becomes

$$\frac{\tau}{\tau_0} \sim \left(\frac{g_0}{g}\right) . \qquad (3\text{-}41)$$

Then for a low-gravity environment of $g/g_0 = 10^{-5}$, Equation 3-41 gives an equivalent time for equal settling of $\tau/\tau_0 = 10^5$. That is to say that for the particles of an LPS to settle an equal distance in a low-gravity environment would require 10^5 as much time as in a one-g environment. Thus, a low-g environment would have a very significant effect on the rate of settling of liquid phase sintered compacts produced in space.

3.4 MODELING OF RELATED EFFECTS

The infiltration of a powdered metal compact is a production technique which is related to liquid phase sintering. In an infiltration process, the pores of a powdered metal are filled with a relatively low-melting liquid metal through the action of capillary forces. In

practice this is accomplished either by heating the compact in contact with the solid infiltrant metal above the melting point of the latter, or by preheating the compact separately and dipping it into the liquid. The liquid, as it sweeps through the circuitous capillary system of the porous body, displaces the gases progressively, thus yielding a relatively dense compact in a short time.

Unlike liquid phase sintering, infiltration involves more directly the classical capillary tube rise phenomena and as such would appear to be much more sensitive to changes in gravity. The maximum height to which a liquid column will rise in a capillary tube is given by

$$h_\infty = \frac{2\sigma_{\ell v} \cos \theta}{r_c \rho \left(\frac{g_0}{g}\right)} \qquad (3\text{-}42)$$

where

- h_∞ - final equilibrium height reached by a liquid column
- $\sigma_{\ell v}$ - liquid/gas surface tension
- θ - liquid/solid contact angle
- r_c - capillary tube radius
- ρ - liquid density
- (g/g_0) - gravitational level.

As can be seen by considering Equation 3-42, the height to which a liquid column would theoretically rise in an orbital environment ($g/g_0 < 10^{-4}$) would be several orders of magnitude greater than the rise height observed in a one-g environment. This leads to the conclusion that significant differences will exist during the infiltration process being carried out

in a one-g and an orbital environment. Semlak and Rhines (Ref. 17) have conducted a study which can be used to show more or less qualitatively how changes in gravity would affect infiltration. The differential equation of motion for a straight capillary tube was derived by Ligenza and Bernstein (Ref. 18) and is

$$\frac{d}{d\tau}\left\{\pi r_c^2\left[\rho h + \rho g\,(\ell - h)\right]\frac{dh}{d\tau}\right\} = 2\pi\, r_c\, \sigma_{\ell v}\cos\theta - 8\pi\,\frac{dh}{d\tau}\left[\mu h + \mu_g\,(\ell - h)\right] - \pi\, r_c^2\left(\frac{g}{g_0}\right) h\,(\rho - \rho_g) - \frac{1}{4}\,\pi\, r_c^2\,\rho\left(\frac{dh}{d\tau}\right)^2 \qquad (3\text{-}43)$$

where

τ - time

ρ_g - density of the gas above the liquid

h - rise height of the liquid column at time τ

ℓ - length of the capillary tube

μ - dynamic viscosity of the liquid

μ_g - dynamic viscosity of the gas above the liquid.

The term on the left of Equation 3-43 represents the rate of change in momentum of the contents of the tube. On the right the terms represent, respectively, the forces due to a) surface tension, b) viscous resistance, c) gravity, and d) entrance drag effects.

Equation 3-43 is not amenable to an explicit solution. However, Semlak and Rhines used a solution applicable to the special conditions where the tube radius is sufficiently small and the rate of rise is slow

enough so that the rate of change in momentum and entrance drag effects may be neglected. Introducing the final boundary conditions and letting the density difference be approximated as $(\rho - \rho_g) \sim \rho$ the solution to Equation 3-43 obtained was

$$\tau = \frac{8}{r_c^2 \rho \left(\frac{g}{g_0}\right)} \left\{ \left[(\mu - \mu_g) h_\infty + \mu_g \ell \right] \ln \frac{h_\infty}{h_\infty - h} - (\mu - \mu_g) h \right\} . \quad (3\text{-}44)$$

By neglecting the viscosity of the gas above the liquid, Equation 3-44 can be reduced to

$$\tau = \frac{8 \mu h_\infty}{r_c^2 \rho \left(\frac{g}{g_0}\right)} \left(\ln \frac{h_\infty}{h_\infty - h} - \frac{h}{h_\infty} \right) . \quad (3\text{-}45)$$

Semlak and Rhines in their study reduced Equation 3-45 further by expanding the log term in a power series and truncating after the second term. However, this approximation eliminates gravity from the resulting equation. By multiplying the straight capillary tube height (h) in Equation 3-45 by a factor of $2/\pi$ to account for the circuitous capillary path of a powdered metal, Semlak and Rhines (Ref. 17) showed that Equation 3-45 gives a good prediction of height rise time for infiltration of powdered metal.

Using the properties for iron being infiltrated by copper as given in Reference 17, Equation 3-45 has been used to compute the effects of small changes in gravity. The results are shown plotted in Figure 3-12. No attempt was made to utilize data resulting from Equation 3-45 for gravity levels less than $g/g_0 = 0.1$ because at low

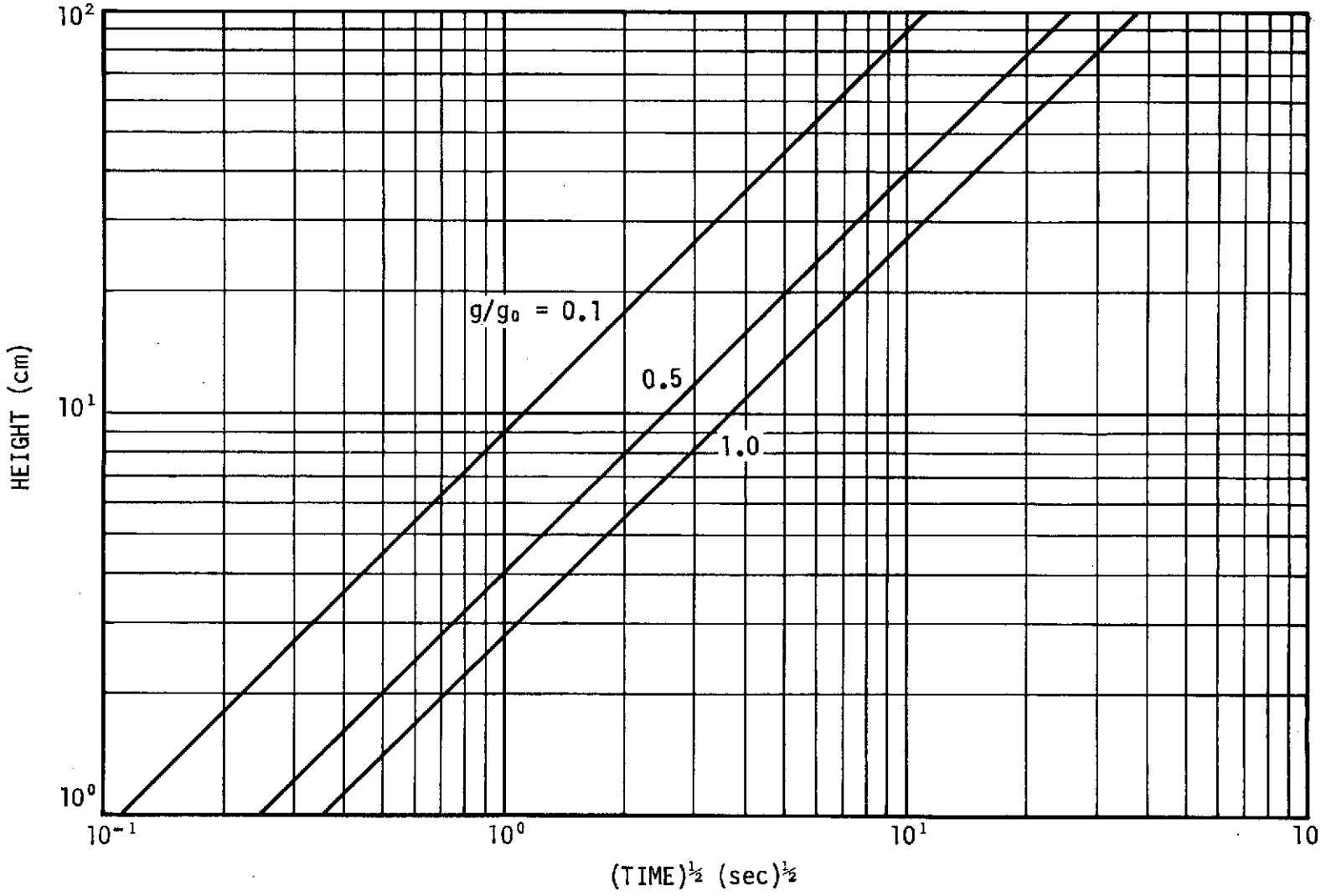

FIGURE 3-12. CAPILLARY HEIGHT RISE TIME AS A FUNCTION OF GRAVITY LEVEL

gravity levels the rate of change in momentum and entrance drag effects cannot be neglected in infiltrating compacts of reasonable size. To determine the effects that low gravity levels would have on the infiltration process would require a numerical solution of Equation 3-43.

The trends and qualitative effects of changes in gravity can be drawn from the results shown in Figure 3-12. From Equation 3-42 it is seen that the equilibrium height to which a column of liquid will rise is a monotonically increasing function of reduced gravity. The results obtained from the approximate equation of motion (i.e., neglecting changes in momentum and entrance effects) show that decreasing gravity tends to increase the infiltration height for a given infiltration time. Likewise the time required to infiltrate to a given height is decreased as gravity is decreased (see Figure 3-12). Thus, it is to be concluded that larger (i.e., dimensionally longer) compacts could be infiltrated in space or that a given compact could be infiltrated in a much shorter time than in a one-g environment. The latter suggests that changes in some of the physical characteristics may also take place as a result of infiltration in a low-gravity environment.

Another attractive aspect of infiltration is that it is a process which would lend itself more favorably to a space experiment. The experimental procedure used by Semlak and Rhines consisted of infiltration of a cylinder of preheated powdered metal. The preheating time varied from a few minutes up to several hours; however, the infiltration time was generally less than 7 seconds. The solidified compact was metallographically inspected to determine physical changes. This short infiltration time would readily lend itself to sounding rocket experiments.

4. EXPERIMENTAL

4.1 MATERIAL SELECTION

The kinetics of sintering and densification depends on the wetting characteristics of the solid phase by the liquid. These two phases show segregation during sintering when the density difference between the two is large. Gravity has influence on both these phenomena. Hence, emphasis was placed on wetting characteristics and density differences when selecting material combinations. Combinations chosen were

- Good wettability with a small difference in density
- Moderate wettability with a large difference in density
- Poor wettability with a large difference in density.

Based on the above, the following material combinations were selected

- 40% by volume Cu + 60% by volume Fe
- 40% by volume Cu + 60% by volume W
- 30% by volume Ag + 70% by volume Al_2O_3.

The relevant properties of these materials are given in Table 4-1.

TABLE 4-1. RELEVANT PROPERTIES

MATERIAL	MELTING POINT °C	DENSITY	SURFACE TENSION		CONTACT ANGLE AT 1100°C
			σ_{SV} erg/cm^2	σ_{LV} erg/cm^2	
Ag	960.8	10.5		940	83°
Al_2O_3	2050	3.5	905		
W	3370	19.3	>2300		35°
Cu	1083	8.92		1270	0°
Fe	1535	7.86	2039		

All these materials were in the form of very fine powders, and all of purity between 99.80 and 99.99 percent. The low-melting materials, i.e., Cu and Ag, had an average particle size of about 40 micrometers. Average particle sizes of 3, 10, and 60 micrometers were used for tungsten, iron, and aluminum oxide, respectively.

4.2 COMPACT FORMATION

The samples of powder combinations were thoroughly blended in a laboratory tumble mill blender with tungsten rod agitators. The blending time was 2 hours in each case.

Both Cu-W and Cu-Fe combinations were reduced in a hydrogen furnace for 5 hours each before blending. This was done to remove any oxide layer buildup on the metal powder surfaces. The reduction was carried out in three heat zones of 940°C, 880°C, and 780°C with 100 minutes of reduction in each zone.

The compaction was carried out in an isostatic pressing unit. The pressures used for Cu-Fe, Cu-W, and Ag-Al_2O_3 systems were 7,000, 15,000, and 30,000 psi, respectively. The compacted samples were cylindrical in shape with approximately 4.5-centimeter diameter and 4.0-centimeter length.

4.3 SINTERING

The compacts were sintered in a vacuum furnace with a protective atmosphere of pure argon, which is passive. This atmosphere was necessary to prevent the evaporation of the liquid phase, which will alter the composition of the mixture and contaminate the furnace system. Steel containers with molybdenum linings were used. The samples were put in the containers with their cylindrical axis vertical

and kept in the vacuum furnace for about 16 hours under a vacuum of 10^{-5} torr. Then the temperature of the furnace was raised to about 300°C under dynamic vacuum and held for about 4 hours. Pure argon was then introduced into the furnace without breaking the vacuum. The furnace was then brought to 1,100°C and held at this temperature for 1 hour. A safety valve kept the pressure in the furnace around atmospheric during the heating cycle. Typical heating time was about 2 hours and the cooldown time was about 10 to 12 hours.

4.4 MEASUREMENTS

Densities of both green and sintered samples were determined and the samples were cut along the cylinder axis and polished. Metallographic photographs and scanning electron microscopy were done on the polished surface. Electrical resistivity mapping of the polished surface was done with a four-point resistivity probe. The variation in the concentration of the liquid phase along lengths parallel to the cylinder axis was determined using atomic absorption spectroscopy.

These experimental techniques will be further elaborated upon in Section 5 under their proper headings.

5. RESULTS AND DISCUSSION

The results obtained through the various types of measurements are discussed in this section. The results are derived from measurements of three batches of the samples. This was done to establish the reproducibility of the sintering procedure.

5.1 DENSITY

The density of the green samples was determined merely by measuring the weight and volume of the sample. Liquid displacement techniques are not recommended since the sample in the green state is quite porous. The density of the sintered samples was determined using fluid displacement techniques. The results of the measurements are shown in Table 5-1. The theoretical density is also tabulated for comparison.

TABLE 5-1. RESULTS ON MEASUREMENT OF DENSITY

SYSTEM	THEORETICAL DENSITY	GREEN DENSITY	SINTERED DENSITY	DENSIFICATION PARAMETER
40% by volume Cu-W	13.184	8.990	8.908	0.0195
40% by volume Cu-Fe	8.252	4.734	7.985	0.9241
30% by volume Ag-Al_2O_3	4.875	3.281		

To avoid the problems encountered because of the variation of green density from compact to compact, a densification parameter P_ρ is defined as

$$P_\rho = \frac{\rho_s - \rho_g}{\rho_T - \rho_g}$$

where ρ_s, ρ_g, and ρ_T are sintered, green, and theoretical densities, respectively.

The calculated densification parameters are shown in Table 5-1.

The Ag-Al_2O_3 system could not be sintered properly under the present experimental conditions. It was possible, though, to compact it properly without any plasticizer, and the green density achieved was 67.3 percent of theoretical density. Such high theoretical density, in general, should give good densification upon sintering.

Observation shows that the sintered part consists of spherical droplets of Ag, of various sizes, scattered around in the matrix of Al_2O_3 (Figure 5-1). The bottom part of the sample is stronger than the top part. The problem in this case is that molten Ag does not wet Al_2O_3 at a contact angle of 83 degrees. Each individual molten particle of the metal thus flows down under the influence of gravity, since Ag is heavier than Al_2O_3 (Table 4-1), joins with other molten particles, and forms a big droplet. This process continues throughout the entire sample until the droplets are so large that they cannot flow any further between the particles of Al_2O_3.

This decreases the concentration of silver in the top part of the sample and the Al_2O_3 particles no longer have any bonding, making the top structure lose its strength. Moreover, the non-wetting characteristics, according to our model, should give a repelling force between the Al_2O_3 particles. This means that, after sintering, there should be a swelling, instead of shrinkage, of the sample. This, however, could not be quantitatively verified, in this case, because the structure could not retain its compacted shape. According to the model, the cohesive force is dependent on both the angle of contact and the quantity of the liquid phase. For the same angle of contact the cohesive force decreases with the increase of the quantity of the liquid phase. This phenomenon is true for spherical particles according to the model, but may be entirely different for particles of other shapes.

FIGURE 5-1. PHOTOMICROGRAPH OF SINTERED Ag-Al_2O_3

The Cu-W system could be sintered under the present experimental conditions; however, it was found that all 40 percent by volume of Cu could not be retained in the sintered body (Figure 5-2). Only about 38 percent by volume of the liquid phase was retained and the rest extruded. The extruded liquid phase suggests that the angle of contact is not 35 degrees as should be for pure liquid Cu and W system and is greater than this, under the present experimental conditions.

This behavior of the Cu-W system could be because of handling of the powder after reduction. The length of time spent for blending, compaction, and transfer to the vacuum furnace was sufficient for the highly active W-powder to pick oxygen from the atmosphere and give it away to the Cu when it melted. This situation with the Cu-W system again verifies the repulsive nature of the cohesive force. According

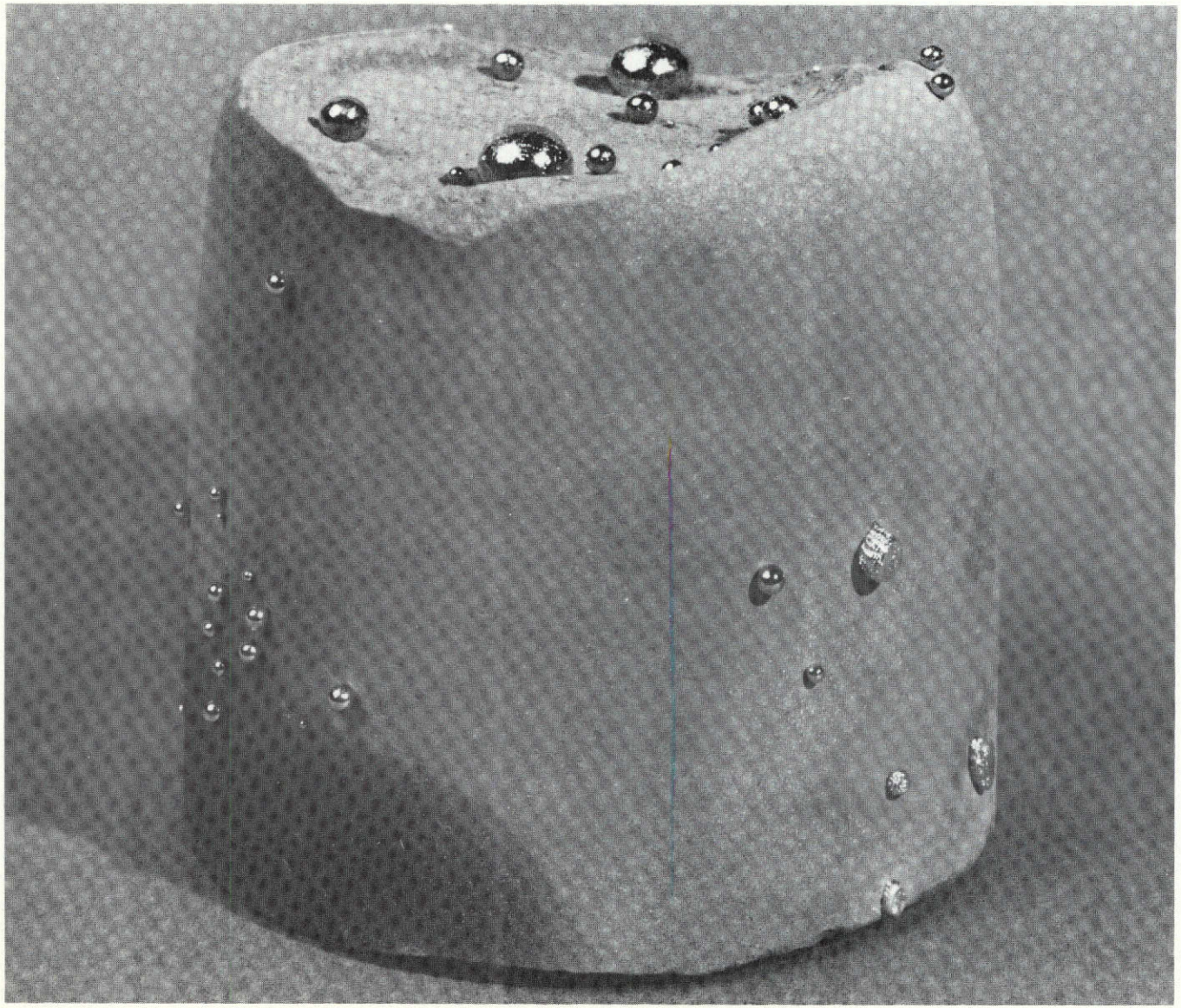

FIGURE 5-2. Cu-W SYSTEM

to the theoretical model, in systems with a large angle of contact the particles are, in general, repelled and there is no shrinkage after sintering. As indicated before, the cohesive force is also dependent on the amount of liquid phase. This prediction of the model is verified through the density measurement. The measured sintered density is lower than the green density (Table 5-1). The green density is 68.2 percent of the theoretical density, whereas the sintered density is only 67.6 percent of the theoretical density. It is possible that 38 percent of liquid Cu gives a very little repelling force under the present modified contact angle condition.

The Cu-Fe system turned out to be the best after sintering. This was expected since liquid copper has a contact angle of 0 degrees with iron. The sintered density is 7.985, i.e., 96.8 percent of the theoretical density as compared to 57 percent for the green. This is in accordance with the model. The model predicts a high attractive force with a contact angle of 0 degrees.

5.2 METALLOGRAPHY

Both the green and sintered samples were cut along the cylinder axis, as mentioned before, and the internal surface thus exposed was polished. Photomicrographs of this surface were taken at a magnification of 200 using a Ziess metallograph. Low magnification was used to reveal the distribution of the two phases in a larger area of the sample.

Scanning Electron Microscopy was then performed on different parts of the sample to determine the variation in the microstructure along the gravity direction.

For the Cu-W system the results of metallography are shown in Figures 5-3 and 5-4. Figure 5-3 is for the green sample and Figure 5-4 is for the sintered sample.

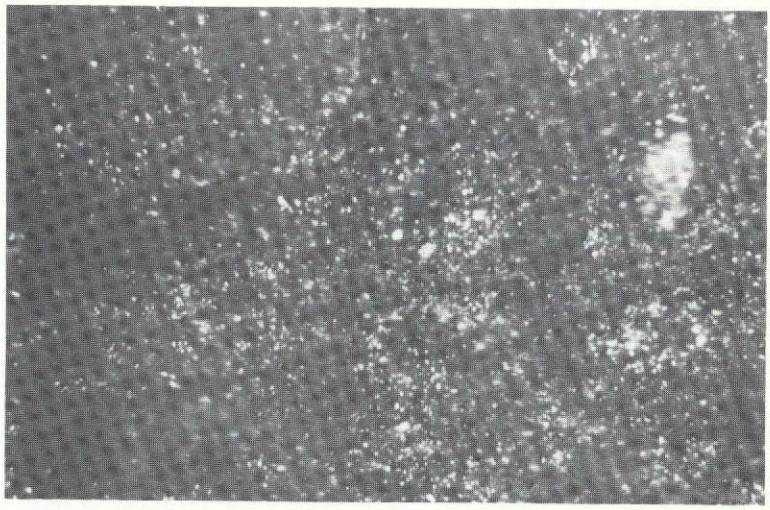

(a) TYPICAL DISTRIBUTION, 200x MAGNIFICATION

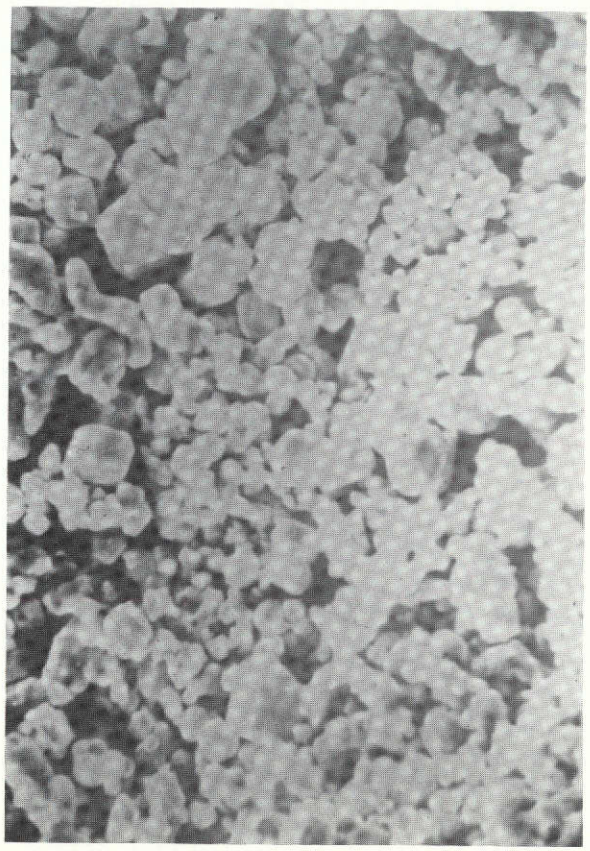

(b) TOP PART OF SAMPLE, 2000x MAGNIFICATION

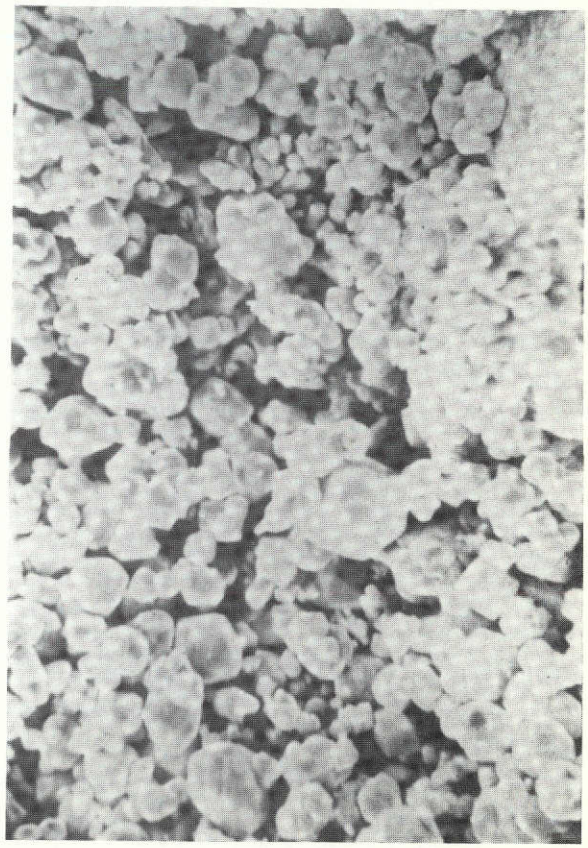

(c) BOTTOM PART OF SAMPLE, 2000x MAGNIFICATION

FIGURE 5-3. PHOTOMICROGRAPH OF Cu-W IN THE GREEN STATE

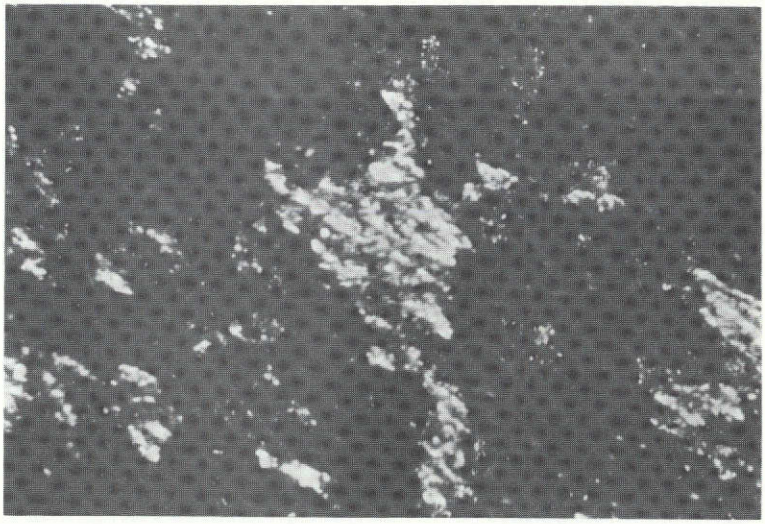

(a) TYPICAL DISTRIBUTION, 200x MAGNIFICATION

(b) TOP PART OF SAMPLE, 2000x MAGNIFICATION

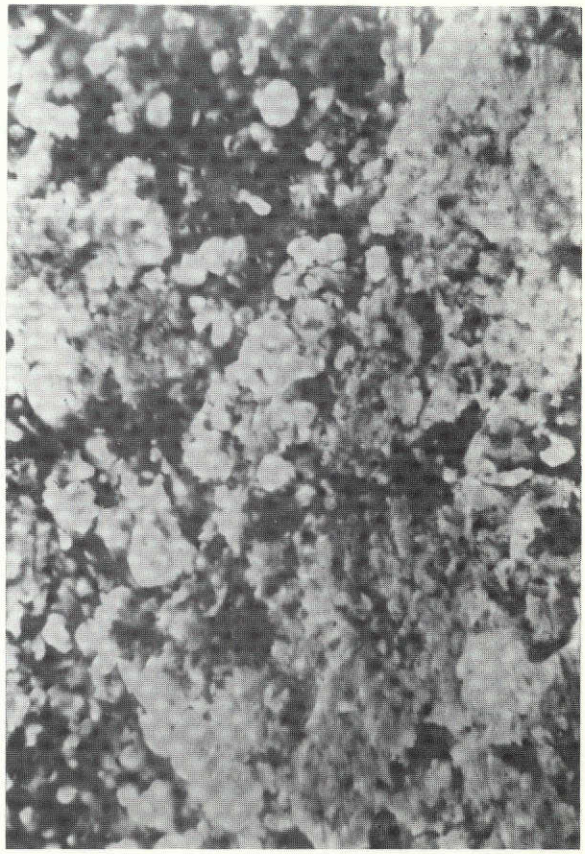

(c) BOTTOM PART OF SAMPLE, 2000x MAGNIFICATION

FIGURE 5-4. PHOTOMICROGRAPH OF SINTERED Cu-W

From a comparison of Figure 5-3a and 5-4a, it is clear that there is migration of the two phases along the gravity direction during sintering. The SEM micrograph of the green compact shows a uniform distribution of the two solids (Figures 5-3b and 5-3c) with small and quite uniformly distributed pores, whereas this is not equally true for the sintered sample (Figures 5-4b and 5-4c). The segregation effect is probably evident because the wetting of the solid phase by the liquid phase is poor and there is a considerable difference between their densities (Table 4-1).

Metallographic results on the Cu-Fe system are shown in Figures 5-5 and 5-6. Again, Figure 5-5 is for the green sample and Figure 5-6 is for the sintered sample.

Figures 5-5a and 5-6a show that the distribution of the two phases is quite uniform along the gravity direction of the sample, both before and after sintering. The distribution after sintering does not seem to be different from the distribution in the green sample. There appears to be a considerable grain growth due to sintering. The distribution of the pores is quite uniform in the green compact which reduces appreciably after sintering as is evident from Figures 5-5b, 5-5c, 5-6b, and 5-6c. This reduction in pore volume and number is evidence of densification as confirmed by density measurements. The segregation effect is not present in this case because the densities of the two solid phases are almost equal (Table 4-1) and there is considerable densification because of high wetting to be expected at the contact angle of 0 degrees.

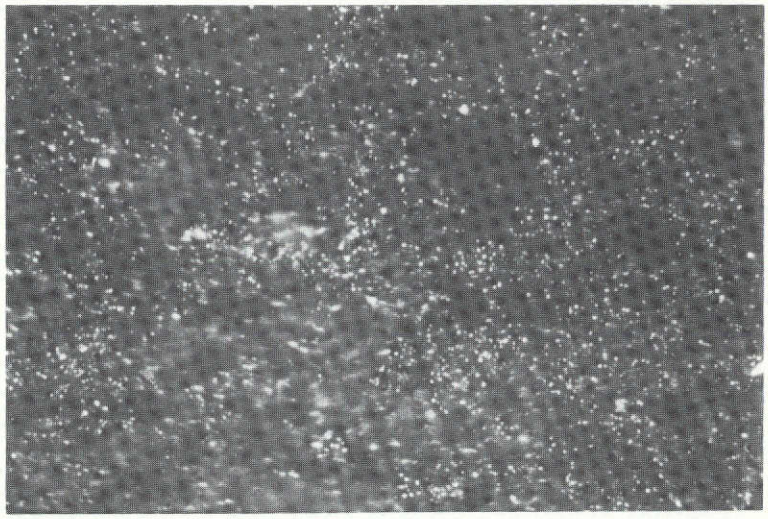

(a) TYPICAL DISTRIBUTION, 200x MAGNIFICATION

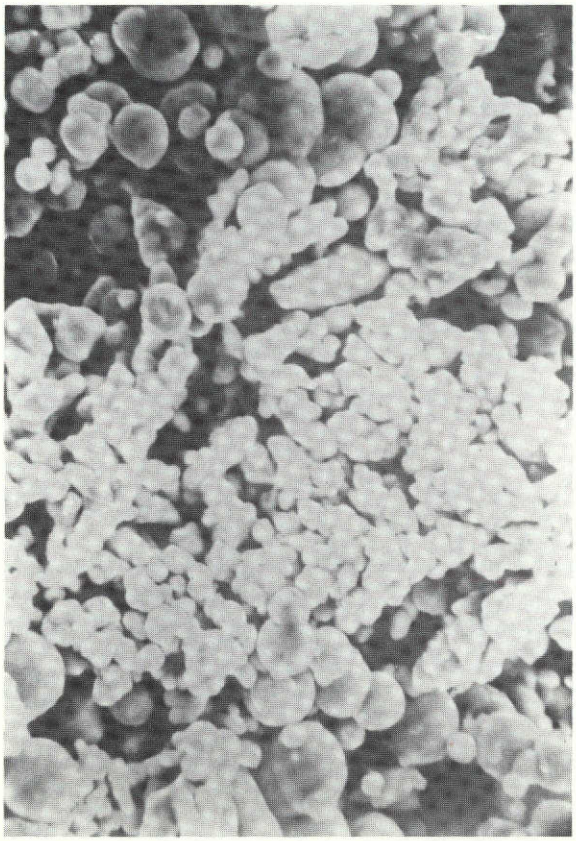

(b) TOP PART OF SAMPLE, 2000x MAGNIFICATION

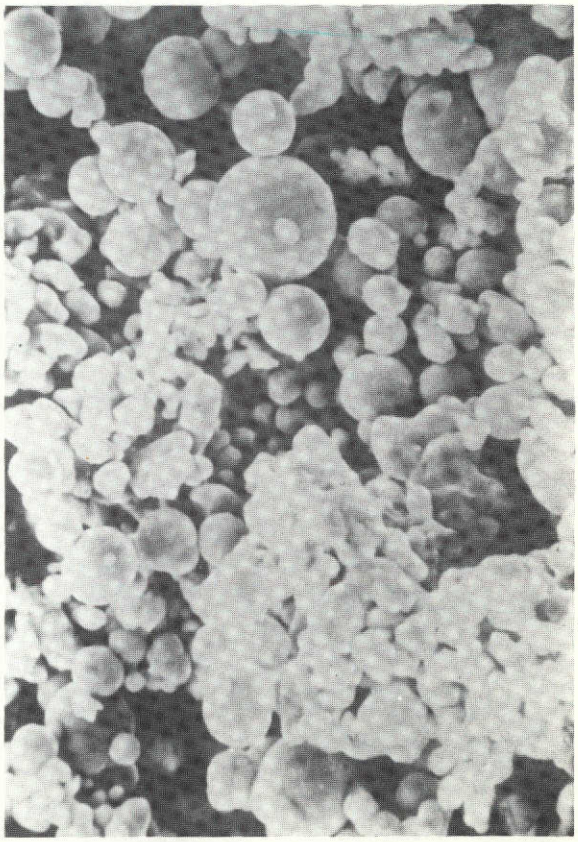

(c) BOTTOM PART OF SAMPLE, 2000x MAGNIFICATION

FIGURE 5-5. PHOTOMICROGRAPH OF Cu-Fe IN THE GREEN STATE

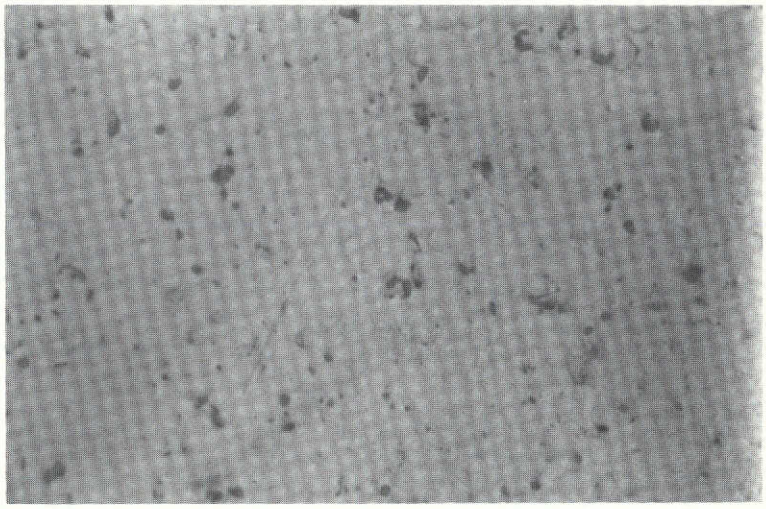

(a) TYPICAL DISTRIBUTION, 200x MAGNIFICATION

(b) TOP PART OF SAMPLE, 2000x MAGNIFICATION

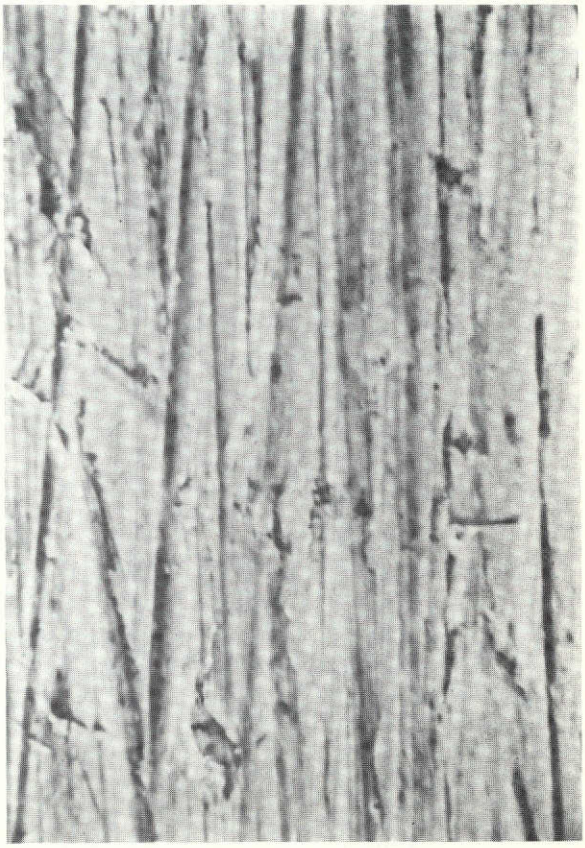

(c) BOTTOM PART OF SAMPLE, 2000x MAGNIFICATION

FIGURE 5-6. PHOTOMICROGRAPH OF SINTERED Cu-Fe

5.3 VARIATION OF COPPER CONCENTRATION

The distribution of copper in the Cu-Fe and Cu-W systems was determined using atomic absorption spectroscopy. This was done to determine the concentration gradient along the gravity direction of the sintered compacts.

Copper concentration was determined using a Perkin-Elmer Model 303 atomic absorption spectrometer. It is a dual-beam system; the monochromator has a high-dispersion Czerny-Turner grating system. The counter readout is in percent absorption.

The results of measurements are presented in Table 5-2. The expected weight percent of Cu in Cu-W and Cu-Fe samples according to the mixture ratio should be 23.07 and 42.85 percent, respectively. For the compacted Cu-W system the experimental result agrees with the calculated value. Also, nearly similar values for the top, middle, and bottom portions of the sample suggest the uniformity of the copper distribution -- suggesting good blending. This uniformity in distribution is disturbed due to sintering. The maximum weight percent difference now increases to 2.9 from 0.3 percent. As can be seen, the copper weight percent is more at all sampling positions than calculated according to mixture ratio. This shows that there was more concentration of copper at these sampling positions and indicates migration of copper due to sintering in the sample. Gravity-driven segregation because of a large difference in density occurs since the wetting is poor. On the other hand, for the Cu-Fe system, the copper concentration in the green sample is always higher than calculated according to mixture ratio and indicates that the blending was not perfect. In spite of this, sintering produced quite uniform distribution of copper in the sample and indicates the absence of segregation in this highly wetting system with a very small difference in density.

TABLE 5-2. WEIGHT PERCENT OF Cu IN SAMPLES

SAMPLE	SAMPLING POSITION ALONG GRAVITY DIRECTION			MAXIMUM WEIGHT PERCENT DIFFERENCE	WEIGHT PERCENT ACCORDING TO MIXTURE RATIO
	TOP	MIDDLE	BOTTOM		
40% Cu + W					23.07
Compacted	23.1	23.1	22.8	0.30	
Sintered	30.4	30.8	27.9	2.90	
40% Cu + Fe					42.85
Compacted	44.1	52.1	43.3	8.80	
Sintered	41.9	41.7	43.5	1.80	

5.4 VARIATION OF ELECTRICAL RESISTIVITY

The surface resistivity of the samples was mapped using a four-point resistivity probe. It consists of a linear array of four tantalum carbide tips of 0.0016-inch radius which are spaced 40 mils from each other. For measurement, the four points are pressed against the surface and a constant current is passed through the outer points. The voltage developed between the two inner points is measured with a sensitive micro-voltmeter.

The results of such measurements on the surfaces of Cu-W and Cu-Fe systems are shown in Figures 5-7 and 5-8. Almost constant resistivity with distance along the gravity direction of the green Cu-W sample (Figure 5-7) shows the uniformity of the distribution of the two components in the sample. The sintered sample does not show the same behavior as the green sample (Figure 5-7). The resistivity along the gravity direction of the sample is no longer as constant as it is with the green. This suggests that segregation has taken place along the gravity direction due to sintering. This supports the finding of other experiments.

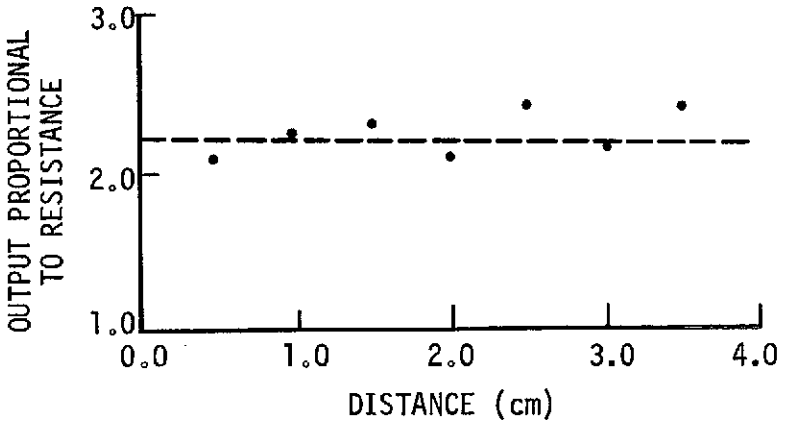

a. Cu + W GREEN

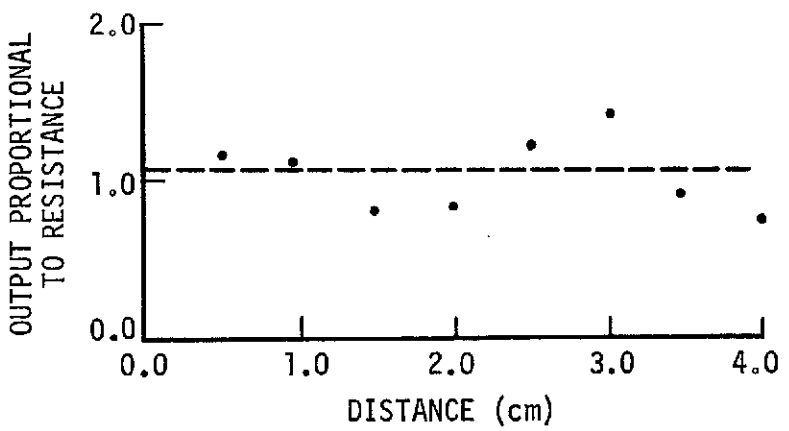

b. Cu + W SINTERED

FIGURE 5-7. VARIATION OF RESISTIVITY WITH DISTANCE FOR THE Cu + W SYSTEM

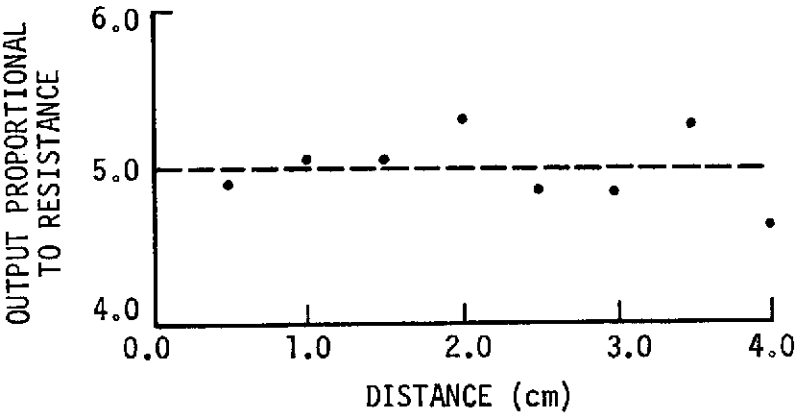

a. Cu + Fe GREEN

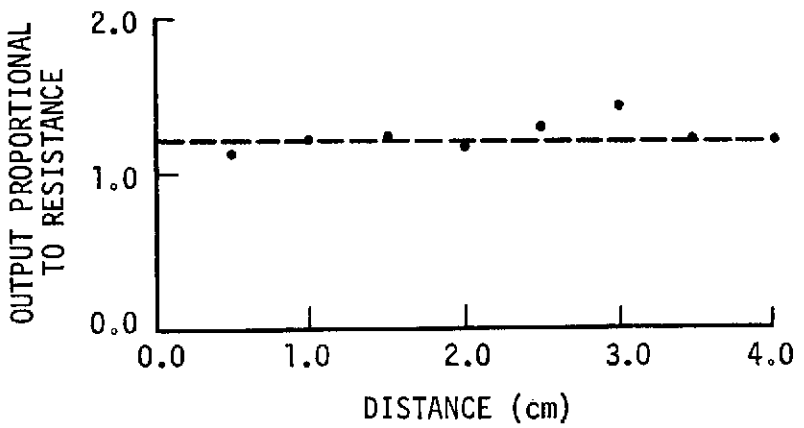

b. Cu + Fe SINTERED

FIGURE 5-8. VARIATION OF RESISTIVITY WITH DISTANCE FOR THE Cu + Fe SYSTEM

The Cu-Fe system, with a very high degree of wetting and small difference in density, does not show a behavior similar to the Cu-W system. In this case the resistivity of the green sample is not as constant as it is for the sintered sample. This shows that the blending of the powders did not produce a good distribution. This situation was, however, improved due to sintering. Sintering improved the distribution of the components along the gravity direction, and no segregation effects were observed. This observation is in line with other observations and supports the theoretical model.

6. DESIGN AND DEFINITION OF SPACE EXPERIMENT

The theoretical model developed and the experimental study performed during this project establishes guidelines to define and design a space experiment to study the effect of low gravity on LPS processes and confirm the validity of the predictions of the theoretical model.

As mentioned before, the theoretical model predicts that the capillary forces acting on the solid-phase particles under one-g conditions are negligibly different from those which will exist under low-g conditions. The segregation effects will be most influenced by low gravity. Two approaches to the design of low-gravity experiments appear to be possible. One, a product approach which will need a long duration of low-g environment; two, a basic approach to study gravity effects on LPS phenomenology, which can be conducted under short duration of low-g.

The selection of materials to study the effect of gravity on the wetting and segregation characteristics associated with LPS is governed by the above two low-g durations. It is necessary to complete all the phases of LPS; i.e., melting, temperature soak, and resolidification; under the same gravity conditions to gather any meaningful result. Hence, the two experiments will be discussed separately.

6.1 LOW GRAVITY FOR LONG DURATION

For this experiment different types of practical materials having manufacturing problems on Earth should be tried. A sample of problem areas where low-g processing might result in improving the process is:

- Infiltration of large objects
- Infiltration of complicated geometry cutting tools
- Segregation in special types of alloys
- Production of high-strength-to-weight ratio composites.

The LPS systems that have been studied under the present contract can be studied under low-gravity and compared with the experiments conducted on Earth. The blending, compacting, and sintering procedures need to be the same for the space experiment as they were for the experiments conducted on Earth. The compacted samples should be put in soft graphite molds. This mold should be put into a stainless steel capsule which should be evacuated. This capsule will then be put in the furnace and the furnace heated to 1,000°C. The "Skylab Multipurpose Furnace" is quite adequate for this. The thermal design of the capsule should be such that every part of the compacted sample gets the same heat. The furnace should be capable of maintaining 1,000°C for at least 1 hour and then turned off. The cooldown time is not critical. The whole process of melting and resolidification should be done free from mechanical disturbance. Experiments which are performed on ground-based samples should be conducted on the space-grown LPS after the capsules are returned to the Earth. These experiments will show:

- The effect of low gravity of the repulsive nature of the cohesive force observed in the Ag-Al_2O_3 system
- Gravity effect on segregation observed in the Cu-W system
- Effect of gravity on grain growth observed in the Cu-Fe system.

It is expected that the Ag-Al_2O_3 system will have no segregation of the two solids and the Cu-W system will produce higher density material with no segregation. It is also possible that the grains in the Cu-Fe system may be larger.

6.2 LOW GRAVITY FOR SHORT DURATION

In this case, material combinations can be selected so that one phase has a very low melting temperature. This will allow the reduction of the melting time. With very low melting materials the melting time could even be reduced to about 1 minute.

The solid phase can be selected from a variety of materials such that the gravity effects on wetting characteristics and density can be studied. In a rocket flight where low gravity is experienced for a short duration of 5 to 7 minutes these materials will allow the study of basic phenomena associated with LPS and the effect of gravity on them. This type of information is necessary to the development of product-oriented flight experiments.

The "Research Rocket Multipurpose Furnace" can be adopted for the suggested LPS work and it has enough capability to perform these experiments and meaningful results can be obtained.

For all material combinations with varying degrees of wetting characteristics and density differences, it is expected that segregation effects will be absent. In the absence of segregation, the low wetting materials will produce homogeneous compacts that would not be possible on Earth. On Earth, the wetting characteristics of low wetting mixtures are increased by techniques such as adding impurities to influence preferential adsorption and/or diffusion fluxes. Wetting characteristics which are basic to LPS are not expected to be affected by gravity, as predicted by the model, and all material combinations with varying degrees of wetting should show the same material properties when compared with Earth-processed compacts.

7. CONCLUSIONS

During sintering there are several separate mechanisms which can operate simultaneously to alter the microstructure of the material. This study has produced the following results with respect to the effect of a low-gravity field on the sintering process.

Since most compacts of interest have liquids with good wetting properties ($\theta < 90°$), surface tension forces and capillary phenomena play a dominant role in changing the microstructure during sintering. Surface tension effects are prominent during both the plastic and liquidus phases. Pores in the material, which are a measure of the degree of densification, appear to be created uniformly throughout the material and become disconnected entities as the liquidus material surrounds the solids. As the sintering process proceeds, the pores shrink in size and/or disappear completely depending upon the degree of solution-precipitation, diffusion and pore surface tension forces. There does not appear to be a significant tendency for the pore (i.e., bubble) to be driven to the surface by gravity-produced buoyancy forces (i.e., at least not in a one-g environment). [The surface tension forces acting to pull the solid particles into closer packing in a one-g environment are not appreciably different from those anticipated in a 10^{-5} g/g_0 (or lower) environment.]

Capillary forces acting on the solid phase particles are dependent on the contact angle and the quantity of the liquid phase.

The cohesive force can be converted to repulsive force by varying the quantity of the liquid phase for certain contact angle values.

Compacts having large amounts of liquid phase and large differences in density between the liquid and solid tend to segregate in a one-g environment as a result of the gravity-driven buoyancy forces. The time for a particle to settle a given amount has been shown to be inversely proportional to the magnitude of the gravitational forces approximately to the first power. Thus, the length of time to produce the same degree of settling in a low-gravity environment will be increased significantly. It appears possible to produce uniform density sintered compacts in a low-g environment which would characteristically exhibit density segregation problems if produced in a one-g environment.

A process which is similar in many respects to liquid phase sintering is the technique of metal infiltration. In this process a strip of low melting material is placed at the top or bottom of a compact made of the high melting component. During sintering the low melting component becomes liquid and is pulled into the compact by capillary forces acting through the circuitous capillary tube system represented by the interconnected voids of the material. Since the height that a liquid will rise in a capillary tube is inversely proportional to the radius of the tube and the gravitational force, changes in these conditions determine the size and shape of compact which can be satisfactorily infiltrated. The equivalent tube radius for compacts is on the order of micrometers, making infiltration a reasonably effective method of filling the voids of the compact. A low-gravity environment would appear to offer a unique means of satisfactorily infiltrating a larger and/or possibly more complex shaped compact.

8. RECOMMENDATIONS

It is recommended that gravity effects on the basic phenomena of LPS be studied using rocket flights which produce low-g for about 5 to 7 minutes. As mentioned above, suitable material combinations can be sought which will have a low melting temperature for the liquid phase and will supply meaningful results on the effect of gravity on wetting characteristics and density segregation, which are basic to LPS.

Gravity is not expected to show any effect on the degree of wetting when compared with Earth-processed LPS compacts. Density segregation in low wetting compacts, which is present in Earth-processed compacts, will be absent in the space-processed materials. This will help in determining if there exists a threshold wetting value beyond which the material has no value even when it may be formed by space processing.

Once enough is known about the effect of gravity on wetting and segregation, it will be possible to define and design product-oriented liquid phase sintering experiments. This will also include infiltration processes. As mentioned before, many product-oriented infiltration processes have problems. Hence, it will be worthwhile to study the effect of low gravity on infiltration processes and find a solution by which infiltration process industries can be helped.

9. REFERENCES

1. Reger, J. L., "AIAA 12th Aerospace Science Meeting", Paper No. 74-207

2. Yaffee, M. L., "Aviation Week of Space Technology", p. 40, February 25, 1974

3. Fabiniak, R., T. Fabiniak, E. C. McKannan, and R. Abbott, "Space Processing and Manufacturing", ME-59-1, 448, October 21, 1969

4. Shaler, A. J., Metals Trans., 185, 796, 1949

5. Mackenzie, J. K. and R. Shuttleworth, Proc. Phys. Soc., B62, 833, 1949

6. Lenel, F. V., Metals Techno., 15, 1, 1948

7. Gurland, J. and J. T. Norton, Jour. Metals, 4, 1051, 1952

8. Kingery, W. D., J. Appl. Phys., 30, 301, 1959

9. Price, T., C. Smithells, and S. Williams, J. Inst. Met., 62, 239, 1938

10. Lenel, F. V., Trans. AIME, 175, 878, 1948

11. Cannon, H. S. and F. V. Lenel, Plansee Seminar Proc. 1952, F. Benesovsky, Editor, p. 106

12. Goetzel, C. G., "Treatise on Powder Metallurgy", Vol. 1, p. 259, Interscience Pub., New York, 1969

13. Hastings, L. J., "Low Gravity Liquid-Vapor Interface Shapes in Axisymmetric Containers", M.S. Thesis, University of Alabama, Huntsville, Alabama, 1968

14. Naidich, Y. V., J. A. Laurinenko, and V. N. Eremenko, International Jour. Powder Metallurgy, 1, 41, 1965

15. Princen, H. M., J. Colloid Interface Sci., 34, 1971, 1970

16. Gorring, R. L. and D. L. Katz, A.I. Ch. E. Jour., 8, 123, 1962

17. Semlak, K. A. and F. N. Rhines, "The Rate of Infiltration of Metals", Trans. of the Metallurgical Soc. of AIME, 325-331, June 1958

18. Ligenza, J. P. and R. B. Bernstein, "The Rate of Rise of Liquids in Fine Vertical Capillaries", Jour. Amer. Chem. Soc., 4636 - 4638, Vol. 73, 1951